2020-01-01

Velocity Measurements Using A Piezoelectric Plate As A Sensor

Paul Perez
University of Texas at El Paso

VELOCITY MEASUREMENTS USING A PIEZOELECTRIC PLATE AS A SENSOR

PAUL ALFREDO PEREZ ITURRALDE

Master's Program in Mechanical Engineering

APPROVED:

Norman Love, Ph.D., Chair

Yirong Lin, Ph.D.

Tzu-Liang (Bill) Tseng, Ph.D.

Stephen L. Crites, Jr., Ph.D.
Dean of the Graduate School

Dedication

I dedicated this work to my parents and siblings because they are the main foundation of my values, they laid my foundations of responsibility and desires for professional improvement.

EXPERIMENTAL SET UP FOR THE TESTING OF A PIEZOELECTRIC MASS FLOW RATE SENSOR

by

PAUL ALFREDO PEREZ ITURRALDE

THESIS

Presented to the Faculty of the Graduate School of

The University of Texas at El Paso

in Partial Fulfillment

of the Requirements

for the Degree of

MASTER OF SCIENCE

Department of Mechanical Engineering

THE UNIVERSITY OF TEXAS AT EL PASO

May 2020

Acknowledgements

This thesis has been funded by National Energy Technology Laboratory (NETL). I would like to thank my examiners, Norman Love, Yirong Lin, and Tzu-Liang (Bill). I am very grateful to my parents for always being there when I need it, thank you for the unconditional support you have given to me to end this part of my life. I appreciated the support of my siblings and perseverance which prompted me to finish this project. I would like to express my sincere gratitude to my advisor Dr. Norman Love for his continuous support, patience, motivation, dedication and for sharing his knowledge with me. He has given to me such a great opportunity and has given me his support on all the programs I have been participated in my career. Thank my coworkers at the University for their support, time and opportunity to develop both personally and professionally.

Abstract

In this study, the voltage output from a piezoelectric sensor placed in a test section is used to predict flow velocity changes. The piezoelectric made of PZT is thought to be advantageous due to its fast response time, potential durability at higher temperatures, and self-powered characteristics. Having said that this sensor could be implemented into the Hybrid Performance Project built by NETL to characterize and mitigate the probability of compressor surge and stall. The problem arises because of the added large volume between compressor and gas turbine and resultant changes to system fluid dynamics. The effect of the piezoelectric sensor shape and the influence of velocity profile on the output voltage is presented in this thesis. In order to test the impact of piezoelectric shape, two different sized piezoelectric made of the same material are used. The impact of velocity profile is determined by exposing the piezoelectric to various velocity profiles with two different test sections. It is found that the voltage increases non-linearly as the velocity is increased for both piezoelectric and for both sets of velocity profiles. The larger piezoelectric, produces significantly more voltage than the smaller piezoelectric. The larger sensor has a maximum output voltage 4.8 times higher than the smaller piezoelectric when subjected to a uniform flow. This has been attributed to the increased size of the sensor that causes more drag force. Drag force is calculated to be 4.5 times greater for the larger sensor. When subjected to a less uniform velocity profile the larger sensor produces more than 120 times more voltage output compared to the small piezoelectric.

Key: Piezoelectric, Flowmeter, Velocity Measurement, Voltage Output

Table of Contents

List of Tables

List of Figures

Chapter 1: Introduction and Background

1.1. INTRODUCTION

In modern power systems, extreme fluctuations of parameters can create events that end up damaging critical system components. Indeed, mechanical properties of components in energy generation systems are sacrificed when the operating parameters fluctuate significantly in areas where sensors may not be positioned. Maintaining an optimum parameter for energy generation systems can be achieved by continuous monitoring of real-time measurement. In fact, operating at optimum parameters leads to enhanced efficiency, accommodates system safety parameters, and maximizes output. Therefore, constant monitoring is essential for optimal functioning and safety of energy systems.(Sarker et al. 2018). For example, Kuchle and Love (Kuchle and Love 2014) and Sarker et al.(Sarker et al. 2018) used thermoelectric and pyroelectric sensors to wirelessly detect temperature inside of a power generation unit at places where thermocouples could not reach. This would allow for real-time health monitoring and material temperatures in places such as turbomachinery of the unit. Other parameters such as velocity may also provide insight into some behaviors of turbomachinery or flow rate within a system. This is particularly attractive if the sensor is capable of detecting rapid changes in the flow or pressure in the area of measurement. Piezoelectrics have been used frequently in the past for pressure measurements. (Hjelmgren 2002) However, flow velocity measurements using the same material are not as well documented in literature possibly due to the nonlinearities between the flow and physical properties of the piezoelectric. Piezoelectric materials have opened so much interest in the area of research. Many studies have been used piezoelectric ceramics as energy harvesting devices [8] – [13]. Energy harvesting piezoelectric capture wind energy, and convert the fluctuations caused by the fluid to electrical current. These devices subject to fluid flow that cause stress and bending on the geometry

that the piezoelectric is attached to. In nearly all cases this motion is converted to electricity. However, the generated signal can also be analyzed to identify flow characteristics such as velocity typically by using soft PZT ceramics. [16], [17]. Previous designs that involve piezoelectric include cantilever beams that vibrate due to vortices produced by fluid flows, such as in a Vortex flow meter (Kim, Kim, and Kim 2011). Many of these sensors in this configuration are also used to harvest energy. [14], [15]. This thesis reviews both piezoelectric energy technologies.

1.2. BACKGROUND ON ENERGY SYSTEMS

A rapidly growing number of people around the world are becoming concerned about environmental issues, including depletion of natural resources, emissions and pollution, deforestation and soil degradation.(Del Rosario 2004) Depending on the electricity source, there can be also environmental challenges. Air pollutants can cause significant harmful negative health impacts. Greenhouse emissions are also an issue. Globally 40% of energy related to carbon dioxide emissions are from electrical generation. Each power plant technology has advantages and disadvantages. For example, nuclear power plants provide large quantities of reliable power with low levels of greenhouse gas emissions, but may not be sustainable over a long period of time. Fossil fuel power plants deliver on-demand, consistent and reliable energy when resources are available. Renewable sources of electricity like solar and wind produce zero direct carbon emissions, but generated electricity on an intermediate or inconsistent basis (“Gas Turbine | Student Energy” n.d.).

Energy harvesting from wasted or unused power has been the topic of discussion for a long period. Cost-efficiency improvements and demand for methods to prevent climate change will increase the implementation of energy harvesting techniques, which can improve overall

efficiency. In recent years, industrial and academic research groups have focused their attention to the problems and limitations of using piezoelectric materials as energy harvesting tools.

1.3. DoE Hyper Facility

Figure 1 presents the Hybrid Performance (HYPER) Project experimental setup built by National Energy Technology Laboratory (NETL) is an experimental setup that utilizes unique technology to meet efficiency and fuel flexibility goals that are required of modern power systems. The recuperated gas turbine cycle is currently the most efficient way to convert thermal energy to electric power. (Tucker, Shadle, and Harun 2017)The coupling of a solid oxide fuel cell (SOFC) and a micro gas turbine is an example of hybrid system where the fuel cell works as thermal source for the gas turbine. A solid oxide fuel cell (SOFC) replaces a conventional combustor, by generating heat that is used to drive a gas turbine and produce electricity. Estimation of cycle efficiency for this system has been placed at around 70% (Zaccaria et al., n.d.)

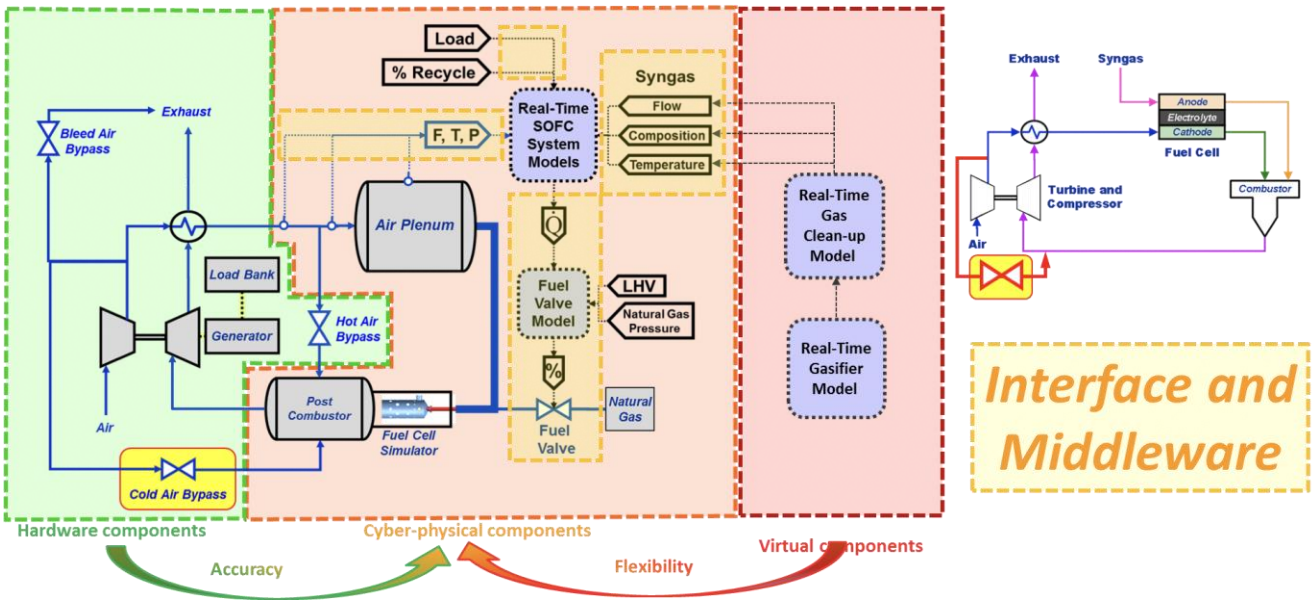

Figure 1The Hybrid Performance (HYPER) Project Diagram (Tucker, Shadle, and Harun 2017)

In this type of system, the air is extracted from the compressor to feed the cathode side of the SOFC. The volume of a hybrid requires two orders of magnitude more than the compressor plenum volume of a simple cycle, which results in a degradation of compressor surge margin and complicated compressor dynamics. When turbine rotational speed is reduced during transients, compressor inlet airflow and pressure ratio decrease at different rates because of the large volume of the system. In this case, the operating point on the compressor map can follow a path toward the stall line. Drastic changes in turbine load or fuel or sudden heat absorption in the fuel cell stack, for example, can thus lead the compressor operation close to stall and surge conditions if not mitigated.(Tucker, n.d.)

1.4. SURGE AND STALL

Surge and stall are one of the main operational challenges in solid oxide fuel cell gas turbine (SOFC/GT) hybrid systems. It occurs when the flow separates from the blades and causes the compressor to stop rotating. Hence, this situation leads to failure of the entire cycle that can be expensive and sometimes impossible to fix and making the industries to invest large amounts of money on reducing or eliminating this from happening. A possible solution is to implement a piezoelectric sensor to identify when surge and stall will occur and stop the process before a catastrophic situation happens.

1.5. PIEZOELECTRIC

The name originates from the Greek word piezo meaning ‘‘pressure’’ and expresses the observation that electricity is generated on applying pressure to a piezoelectric material. The phenomenon response is called piezoelectricity. It is described as the relation between mechanical and electric fields response of piezoelectric materials. A mechanical effect such as strain results in

an electric output like potential, this is called direct piezoelectric effect, which is the basis for piezoelectric sensors.

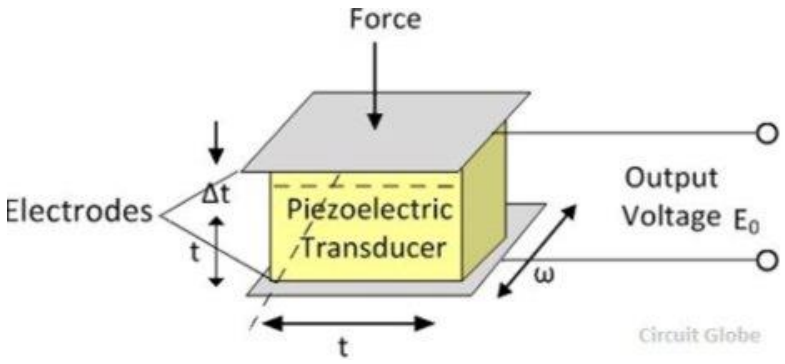

Figure 2 Direct piezoelectric effect ("What Is Piezo-Electric Transducer? - Definition, Piezo-Electric Effect, Theory, Properties & Uses - Circuit Globe" n.d.)

The inverse which is a mechanical output due to an applied electric effect such as voltage, is called converse piezo electric effect. This phenomenon was first discovered in 1880 when Curie's brothers demonstrated that when prepared crystals were subjected to a mechanical stress, they could measure a surface charge. A year later, Lippmann deduced from thermodynamics that they would also exhibit a strain in an applied electric field. The Curies later experimentally confirmed this effect and provided proof of the linear and reversible nature of piezoelectricity.

In general, piezo ceramics are the preferred choice because they are physically strong, chemically inert and relatively inexpensive to manufacture. Plus, they can be easily tailored to meet the requirements of a specific purpose. Piezoelectric materials reveal a unique range of properties and amazing characteristics to produce electricity. Due to the research done on these materials, today there is a wide range of piezoelectric materials to choose from. The Piezoelectric material chosen for testing in this study was based on the operating temperature and performance of the sensor among other things. Lead Zirconate Titanite (PZT) could easily meet the requirements because of its properties and characteristics. PZT was developed around 1952 at the Tokyo Institute of Technology. PZT ceramic is special because it has an even greater sensitivity

and higher operating temperature than other piezo ceramics. In comparison to the previously discovered metallic oxide based piezoelectric material Barium Titanate ($BaTiO_3$), PZT materials exhibit greater sensitivity and have a higher operating temperature.

Factors considered while choosing the piezoelectric materials were:

1. The electromechanical coupling factor k
2. Piezoelectric strain constant d
3. Piezoelectric voltage constant g
4. Mechanical quality factor QM
5. Acoustic Impedance Z
6. Piezoelectric operating temperature

1.5.1. Using Piezoelectric Materials as Energy Harvesters

Energy harvesting is defined as capturing amounts of energy from one or more of the surrounding energy sources, accumulating them and storing them for later use. In other words, harvesting energy from ambient vibrations to convert it into electrical energy is possible using piezoelectric elements. The energy can be stored and used to bias low power electronic devices. With recent advances on wireless and MEMS technology, energy harvesting is highlighted as the alternatives of the conventional battery. Ultra-low power portable electronics and wireless sensors use the conventional batteries as their power sources, but the life of the battery is limited and very short compared to the working life of the devices. The replacement or recharging of the battery is inefficient and sometimes impossible. Therefore, a great number of researches have been focusing on the energy harvesting technology as a self-powered source of portable devices or wireless sensor network system. Piezoelectric materials are a convenient way to extract energy

from vibrating structures. Because these materials exhibit electro- mechanical coupling, they can convert strain energy to electrical energy and vice versa. Piezoelectric materials have found wide application as low power generators. In the majority of these applications, the energy harvester is attached to a structure, and it extracts energy from ambient vibrations by operating as a base-excited oscillator. Several analytical models have been proposed to quantify the electrical energy that can be generated. Ambrosio et al(Ambrosio et al. 2011) proposed a lead zirconium titanite cantilever as a power generator to an energy harvesting system. The optimal performance is determined in terms of power output. Two different configurations of the piezoelectric element were studied: series and parallel. The maximum output power produced by the piezoelectric system was 120 mW at the operating frequency of 40 Hz across a resistive load of 70 kΩ. The useful power was capable to bias some electronic devices. Čeponis et al(Čeponis et al. 2018) demonstrated results of numerical and experimental investigation of trapezoidal cantilevers with irregular cross-sections. Modifications of the cross-section were made in order to increase strain and improve its distribution in the piezo ceramic layer of a cantilever. The numerical investigation showed a dependency between strain and electrical output of the piezoelectric sensor geometry. Other important results showed that the generated electric power for a geometry modified piezoelectric cantilever is more than 11.5-times greater than the power obtained from the conventional cantilever. Choi et al. (Choi et al. 2006) developed an energy harvesting MEMS device using thin film PZT to enable self-supportive sensors. Resonating at specific frequencies of an external vibrational energy source can create electrical energy via the piezoelectric effect. The effect of proof mass, beam shape and damping on the power generating performance were modeled to provide guideline for maximum power harvesting from environmentally available low frequency vibrations. Sirohi et al(Sirohi and Mahadik 2011)

developed a device based on a galloping piezoelectric bimorph cantilever beam to extract power from wind. The beam has a rigid, prismatic tip body of D-shaped cross section. Piezoelectric sheets bonded on the beam convert the strain energy into electrical energy. The power output was observed to increase rapidly with increasing wind speed. Due to the structural damping of the beam, a minimum wind velocity of 2.5 m/s was required to generate power from this device. A maximum power output of 1.14 mW was measured at a wind velocity of 4.7 m/s. Weinstein. (Weinstein et al. 2012) proposed a cantilevered piezoelectric beam in a heating, ventilation and air conditioning (HVAC) flow. The geometry consists of a fixed cylinder and a bilayer cantilever with one end clamped on the cylinder and the other end free. The fixed cylinder is used to generate vortex street. The positioning of small weights along the fin enables tuning of the energy harvested. Power generation of 200 μW for a flow speed of 2.5 m/s and power generation of 3 mW for a flow speed of 5 m/s was achieved. Power output from this device was between 100 and 3000 μW for flow speeds in the range of 2–5 m/s. These power outputs are sufficient to power a wireless sensor node for HVAC monitoring systems or other sensors for smart building technology. Shen et al.(Shen et al. 2008) proposed a PZT piezoelectric cantilever with a micromachined Si proof mass for a low frequency vibration energy harvesting application. The average power and power density were 0.32 W and 416 W/cm^3.

1.5.2. Using Piezoelectric Materials as Flow Rate Sensors

Many previous studies have demonstrated the successful application of MEMS techniques to the fabrication of a variety of flow sensors. According to a previous study, Liu et al. (Liu et al. 2012) used a Lead Zirconium titanite (PZT) microcantilever as an air flow sensor

and for wind-driven energy harvesting. They obtained flow sensing sensitivity of 9 mV/ (m/s). With a 100 kΩ load the sensor produced 18.1 mV and 3.3 nW at a flow velocity of 15.6 m/s. Young et al. (Seo and Kim 2010)proposed a self-resonant flow sensor based on a resonant frequency shift due to turbulence-induced vibrations. The response of the cantilever beam was modulated with its own resonant frequency. The flow drag force induced a mechanical strain on the cantilever beam, and then, the modulated frequency shifted. The device is a dangling crossflow stalk, which can amplify the vibration by an order of magnitude. The experimental demonstration showed a peak output power of 0.6 mW and max power density of 2 mW/cm^3. Yu-Hsiang et al. (Wang, Lee, and Chiang 2007) has developed a MEMS-based air flow sensor featuring a free-standing micro-cantilever structure. In the sensing operation, the air flow velocity is detected by measuring the change in resistance of a piezoelectric layer deposited on a cantilever beam as the beam deforms under the effect of the passing air flow. The experimental results indicate that the flow sensor has a high sensitivity ($0.0284\ \Omega/ms^{-1}$), a high velocity measurement limit ($45\ ms^{-1}$) and a rapid response time (0.53 s). Qi Li. et al (Li et al. 2019) proposed a method to measure the flow velocity of a fluid without affecting its motion state, this method was based on a polyvinylidene fluoride (PVDF) piezoelectric film sensor. The piezoelectric principle of a PVDF film was analyzed, the turbulence noise of a flat-panel model was simulated, a flow velocity measurement system with a PVDF film as the sensing component was built, and the piezoelectric response of the PVDF sensor under wind excitation was measured. The proposed method was shown to be reliable and effective.

1.6. THESIS OBJECTIVE

The objective of this thesis is to design a piezoelectric sensor that can relate changes in voltage output to various fluid velocities. The voltage output of the sensor will be calibrated and used to measure fluid velocity for 1-D flow. The tasks needed to complete the objective for this thesis are listed below:

Task 1: Design a system that can be used to produce repeatable flow velocities and that is capable of controlling air flow velocities from 0-15 m/s.

Task 2: Measure voltage output from sensor when exposed to multiple fluid velocities at room temperature and pressure.

Task 3: Calibrate sensor voltage output with fluid velocity magnitude

Task 4: Design a piezoelectric sensor that meets the design requirements for implementation into a larger external system (NETL Hyper Facility)

1.7. PRACTICAL RELEVANCE

Improving the overall efficiency of The Hybrid Performance (HYPER) system may be achievable through the integration of a sensor, such as the one proposed. Compressor surge is not only destructible for the turbomachinery, but also extremely harmful for the fragile SOFC electrolyte. Hence, compressor dynamics need to be adequately controlled, and a safe emergency system needs to be implemented on this type of power plants to avoid surge during sudden maneuvers such as emergency shut down. The challenges illustrated and discussed are applicable to any gas turbine-based hybrid system where a substantial volume is added between compressor and expander, such as concentrated solar gas turbine hybrid plants, integrated thermal energy storage gas turbine system, and integrated geothermal gas turbine hybrids.

If the compressor dynamics could be controlled at a rate that is faster than existing hardware allows, compressor surge may be detected and avoided before causing damage. The operation of the HYPER facility may be improved, and compressor stall be mitigated during periods of transient operation if a rapidly responding measurement sensors is integrated. Investigating the use of piezoelectric sensors for a variety of power generation monitoring applications. Recent work has demonstrated the ability of a sensor to be used in a wireless configuration to measure pressure change using a lower temperature material, Lead-Ziroconate Titanate (PZT). In fact, developing a sensor that is capable of measuring instantaneous pressure measurements would prevent these challenges. The sensor could be placed on the surface of the measurement point of interest. Once in place, the material generates a current when exposed to a pressure change with time. The current generated by the sensor can be calibrated to represent changes in pressure or wind and control the system.

Chapter 2: Methodology

2.1. DESCRIPTION OF THE EXPERIMENTAL DESIGN PROCESS

Two different setups were used for this thesis in order to determine the effect of the shape of the piezoelectric and velocity profile impacting the ceramic sensor. The following sections describe of the experimental setups used.

2.1.1. Rectangular Test Section (RTS) Setup

Figure 3 shows the various components of the rectangular test section setup. Fans are connected to the test section though a reduction coupling and flow delivery tubes. They generate air flow velocity at room temperature ranging between 0 to 15 m/s. Air flow is passed through a flow strainer located at the base of the pipe to insure uniaxial flow. Finally, the air enters the test section where it interacts with the piezoelectric test article. The piezoelectric is attached to mount

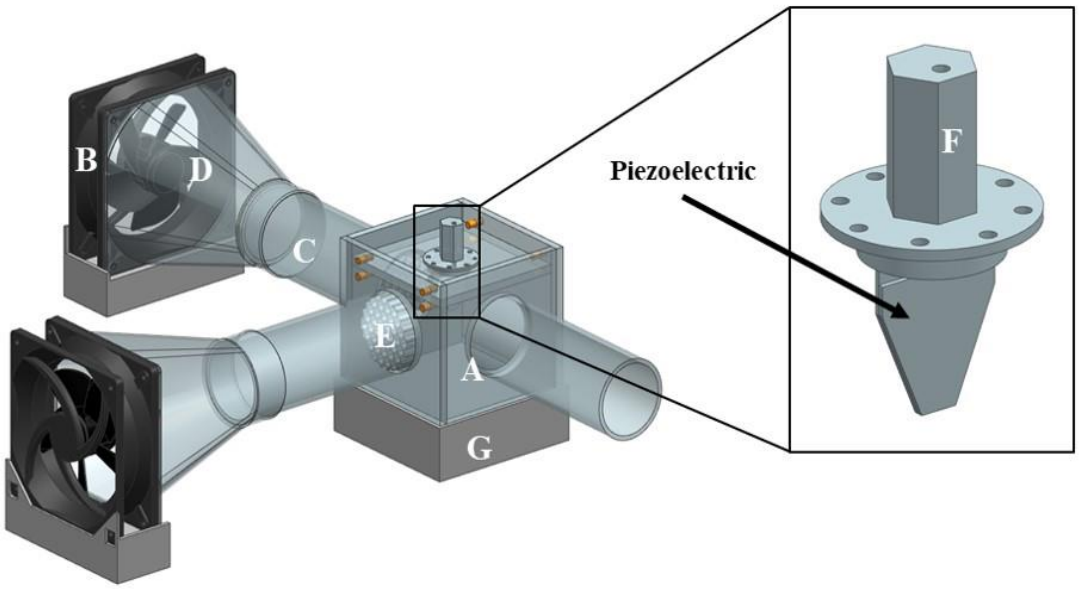

A	B	C	D	E	F	G
Test chamber	DC Axial Fans	Delivery Tube	Reduction Coupling	Flow Straightener	Sensing Element & mount	Support

Figure 3 Experimental apparatus with rectangular test section (RTS)

at the center of the test section and bolted into place. The drag force and pressure differences occurring in the test section cause the piezoelectric to vibrate and generate stress that results in a voltage output from the sensing element. This voltage is measured and recorded using an oscilloscope, RIGOL DS1102E.

The rectangular test section consists of 6 acrylic walls with a thickness of 0.6 cm. The outer dimensions of the cube are 10 x 10 x 10 cm. Three of the side walls have a 5.72 cm diameter hole in the center for air flow. Two of ports are used for inlet flow and they are adjacent to each other, while the other is used for an outlet. For this study only two of the three ports are used, corresponding to C and A in Figure 3. The third port is plugged so as to only allow flow in one direction relative to the sensor. The top wall is adjustable in height, and it is held in place by pins that are inserted in two of the side walls. The set height for the test chamber for this thesis is 8 cm. The top wall has 1.8 cm diameter port at the center to insert the sensor mounting connected to the piezoelectric sensor. The mounting of the sensor is made of polylactide (PLA).

The diagram of the experimental setup for the resting of a piezoelectric flow meter sensor is presented in figure 4. The physical configuration of the axial compact fan follows the diagram schematic.

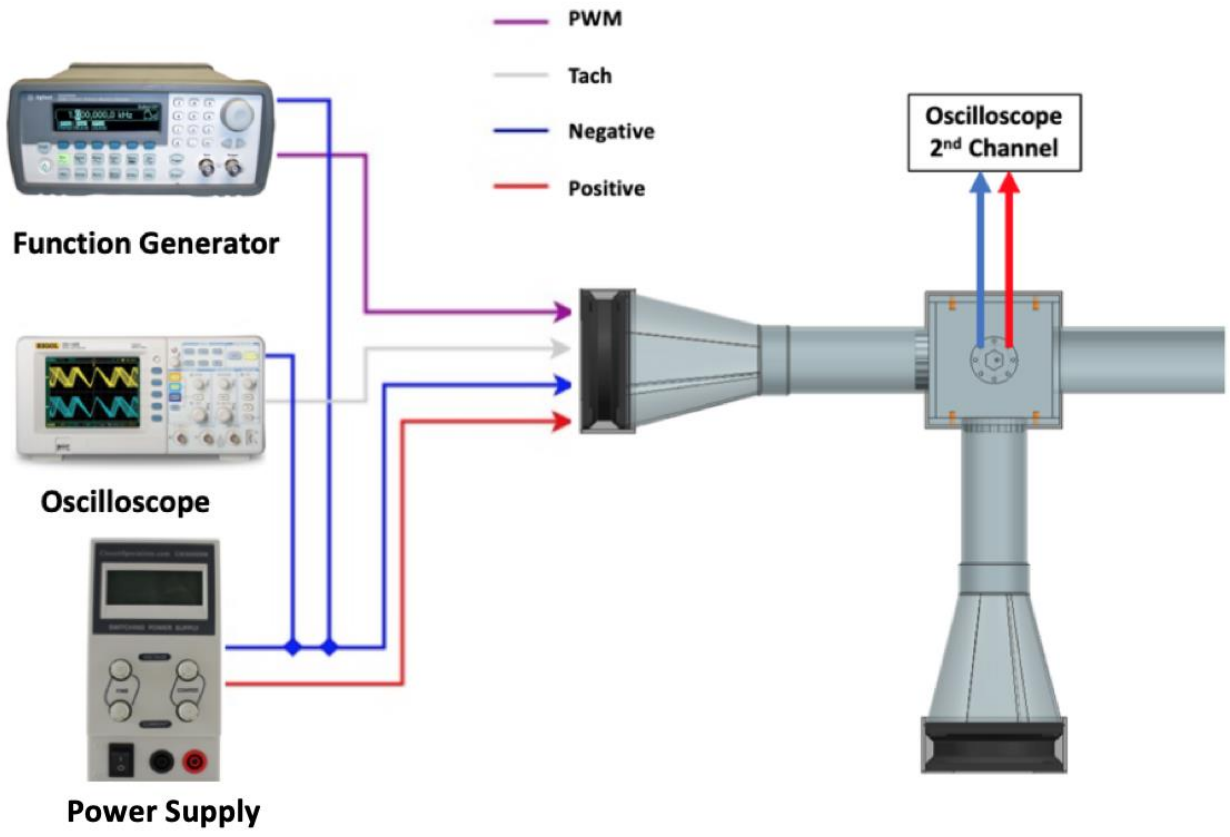

Figure 4 RTC layout and control schematic

For this study the sensor is always placed perpendicular to the flow. A DC axial fan with a nominal voltage of 24V, capable of running from 0-9500 RPM provides the air flow. The fans are powered by a power supply. Each fan is connected to the test chamber through an acrylic tube and a reduction adapter that allows the flow to go from the fan to the chamber inlets through the tubes. The generated signal is measured and acquired by an oscilloscope.

2.1.2. Circular Test Section (CTS) Setup

Figure 5 presents the laboratory scale wind tunnel used for experimentation. The wind tunnel has a 10 cm diameter test section. The piezoelectric sensors are placed into the test section and exposed to the fluid. Air is used as the working fluid for the current experiments at a controlled flow rate. The piezoelectric sensing element is mounted on a holder and placed into the wind tunnel test section. The piezoelectric is fixed on one end of the mounting and allowed to be free on the other end of the mounting. The positioning of the piezoelectric is maintained perpendicular to the air flow for all tests presented in this study. Similar to the RTC, an oscilloscope is used to collect the signal elements.

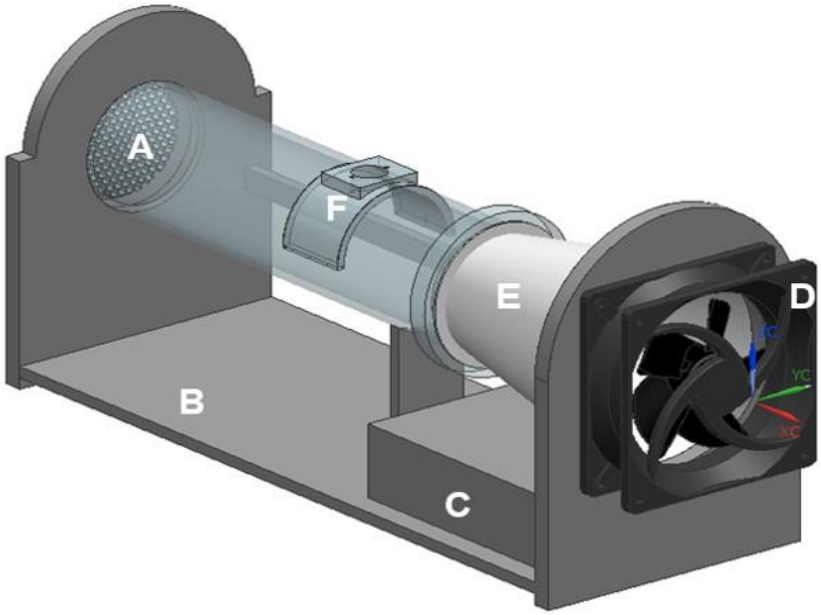

A	B	C	D	E	F
Flow Straighter	Base	Controller	DC axial fan	Reduction coupling	Sensing element and mount

Figure 5 Experimental apparatus with circular test section (CTS)

The flow rate is driven by a fan, by manipulating the fan speed, the flow velocity is varied at average velocities of 2, 4, 9, and 14 m/s for states 1,2,3, and 4, respectively. These values are based on preset fan control settings.

2.2. LIST OF INSTRUMENTATION

2.2.1. DC Axial Compact fan

Figure 6 DC Axial Compact Fan

An axial fan is a type of fan that causes a fluid to flow through it in an axial direction, parallel to the shaft about which the blades rotate. The flow is axial at entry and exit. The fan is designed to produce a pressure difference to cause a flow through the fan. A 4-WIRE fan has power, ground, and tach signal which provides a signal with frequency proportional to speed, a PWM input, which is used to control the speed of the fan. Instead of switching the power to the entire fan ON and OFF, only the power to the drive coils is switched, making the tach information available continuously. PWM, in brief, uses the relative width of pulses in a train of on-off pulses to adjust the level of power applied to the motor. Another advantage of 4-wire fans is that the fan speed can be controlled at speeds as low as 10% of the fan's full speed. A 4114 N/2H7P DC Axial compact fan is used as it provides all characteristics need it for the experimental setup. It is a clockwise rotor fan and its speed control range vary from 500 rpm-1 up to 950 rpm-1. At 0% PWM, maximum speed if control cable (PWM) is interrupted.

2.2.2. Power Supply

Figure 7 Power supply

The CSI3005SM is a compact benchtop linear power supply. For applications that require a decent amount of clean power this unit can deliver up to 30 volts and 5 amps. The current and voltage output can be preset by the user via two sets of multi-turn knobs that offer coarse and fine adjustment for precise settings. Power supply provides constant power to the DC Axial fan of 24V.

2.2.3. Function Generator

Figure 8 Function Generator

A function generator is a piece of electronic test equipment or software used to generate different types of electrical waveforms over a wide range of frequencies. Some of the most common waveforms produced by the function generator are the sine wave, square wave, triangular wave and sawtooth shapes. The Agilent Technologies 33210A used creates stable, accurate low distortion sine waves as well as square waves with fast rise and fall times up to 10 MHz and linear ramp waves up to 100 kHz. The square wave is a special case of a pulse wave which allows

arbitrary durations at minimum and maximum. The ratio of the high period to the total period of a pulse wave is called the duty cycle. Using the apparatus, the fans duty cycle can be control ranging from 20 to 100 % meaning an increment or decrease on the RPM's of the fan.

2.2.4. Hotwire Anemometer

Figure 9 HWA2005DL Hot Wire Anemometer with Real-Time Data Logger

The anemometer used in this study provides multiple features that make it suitable to use in such applications as environmental testing, balancing of fans/motors/blowers, air conveyors, clean rooms, and flow hoods. The apparatus measures velocity, and air temperature, and has an input socket that accepts a Type J or K thermocouple that can be used as a highly accurate thermometer. The integrated hot wire and standard thermistors provide fast and accurate readings-even at low velocities.

2.2.5. Oscilloscope

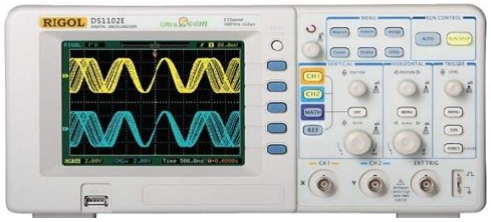

Figure 10 Oscilloscope

A RIGOL DS1102E oscilloscope is used to display and analyze the waveform of electronic signals. In effect, the device draws a graph of the instantaneous signal voltage as a function of time. In any oscilloscope, the horizontal sweep is measured in seconds per division, and the vertical deflection is measured in volts per division. It has multiple inputs, called channels, and each one of these acts independently. The oscilloscope has a sampling rate of 1GSa/s maximum real-time sample rate and 25GSa/s maximum equivalent sample rate, with Bandwidth of 100MHz per channel. Also, it has a maximum 16k- point normal record length and one million points on maximum record length.

Table 1 Oscilloscope configuration

Channel Mode	Sample rate	Memory Depth (normal)	Memory Depth (long record)
Single channel	1GSa/s	16kpts	N.A.
Single channel	500MSa/s or lower	16kpts	1Mpts
Dual channel	500MSa/s or lower	8kpts	N.A.
Dual channel	250MSa/s or lower	8kpts	512kpts

The oscilloscope can be adjusted so that repetitive signals can be observed as a continuous shape on the screen. Using real-time sampling configuration, the oscilloscope samples the waveform often enough that it captures a complete image of the waveform with each acquisition. Utilizing the long memory, the oscilloscopes can capture complex signals in great detail over extended time periods. This allows an observer to examine high frequency effects within the captured waveform. Typically, when multiple channels are in use, the sample rate is split up among the channels. The Nyquist Sampling Theorem, named after Harry Nyquist, who laid the groundwork in 1928, states that in rendering an analog signal as digital data, the sampling rate must be greater than at least twice the frequency of the analog signal. This is called the Nyquist Frequency. If this criterion is not met, aliasing may arise. That is because at a sampling rate that is less than twice the frequency of the signal under investigation, ambiguous results may appear in the form of errors in the display. These aliases can be eliminated by choosing a sampling rate that is appropriate to the frequency of the signal being viewed.

$$\boldsymbol{F_{sampling} \geq 2F_{signal}}$$

Bandwidth and record length are being modified to optimize the oscilloscope's performance. Bandwidth is the single most important characteristic of an oscilloscope, as it gives an indication of its range in the frequency domain. In other words, it dictates the range of signals (in terms of frequency measured in Hertz) that you are able to accurately display and test. Without sufficient bandwidth, the oscilloscope will not display an accurate representation of the actual signal. With too much bandwidth, it will capture excessive noise, providing you with an inaccurate measurement. The bandwidth of an oscilloscope is the lowest frequency at which an input signal is attenuated by 3 dB. The oscilloscope has two options for bandwidth ON and OFF, setting up

bandwidth limit to “OFF” status. The oscilloscope is set to full bandwidth and passing the high frequency component in the signal. On the other hand, setting up bandwidth limit to “ON” status. It will reject the frequency component higher than 20MHz. For digital applications, you should select a scope that has a bandwidth that is at least five times higher than the fastest clock rate in your design. But if accurate edge-speed measurements on the signals, determinizing the maximum practical frequency present in your signal will be need. For analog applications, select a scope that has a bandwidth that is at least three times higher than the highest analog frequency of your designs.

The RIGOL DS1102E has a sampling rate of 1GS/sec. Each second, the scope takes one billion samples of an analog electrical signal to create the digital version. It is clear that the greater the samples per second, the more clearly and accurately the waveform is displayed. However, sampling rate is a fixed amount (set by the record length divided by the time captured). It is given in the specifications for a particular oscilloscope and cannot be changed by the user. However, it may drop because of memory constraints, depending on the frequency of the signal of interest. If we kept increasing the sample rate for the waveform in this above example, the sampled points would eventually look almost continuous. In fact, oscilloscopes usually use sin(x)/x interpolation to fill in between the sampled points. Memory Depth places an upper limit on the number of samples that can be stored in a digitizing oscilloscope. Two relationships are relevant in this discussion:

Sample Rate = Record Length/Time Duration

Time Duration = Record Length/Sample Rate

Record length is expressed in total points or samples. At a low record length, the display would be less informative. Record Length has two alternate values, The maximum record length and normal length. The sample rate is determined solely by the ratio of the record length and the length of the horizontal scale. For this reason, the various record length options let the user adjust the sample rate indirectly. A higher record length gives a better representation of the signal but does not always equate to the highest sample rate. In fact, it takes a faster sample rate to capture some signals. However, when there are not enough samples, the accuracy of the measurement could degrade. Always, trying to avoid aliasing, the Nyquist ratio must be observed. So, between representation and resolution, there is a choice to be made.

Record Length refers to exactly how many samples or points and, therefore, what length of time can be stored. The sampling rate decreases as you increase the range of time. Record Length is important because the more memory depth an oscilloscope has, the more time you can spend capturing waveforms at full sampling speed. Mathematically, this can be seen by:

Record Length = (sample rate) (Time Duration)

So, looking at long periods of time with high resolution between points, deep memory will be needed. It must be required a sample rate that will provide enough detail to see any unexpected glitches or anomalies. Utilizing the long memory, RIGOL scopes can capture complex signals in great detail over extended time periods. This allows an observer to examine high frequency effects within the captured waveform. For the data analysis, data is imported from the oscilloscope and then transferred to MS Excel, it will be then used to analyze the measurement data obtained from the experiment.

2.2.6. Piezoelectric Sensors

Two types of piezoelectric sensors are used in this study and are made from Lead Zirconate Titanite (PZT) falling into two broad categories. The first piezoelectric sensor called hard piezo ceramic is ideal for many high-power applications, while the other is soft piezo ideal for many sensing applications. Table 2 is the comparison between soft and hard ceramic. A larger piezoelectric, constants higher permittivity, larger dielectric constants, higher dielectric losses, larger electromechanical coupling factors, low mechanical quality factors, lower coercive field, poor linearity and is easier to depolarize. ideal for many sensing applications.

Table 2 Comparison between soft and hard piezo ceramics

Characteristic	Soft Ceramic	Hard Ceramic
Piezoelectric Constants	larger	smaller
Permittivity	higher	lower
Dielectric Constants	larger	smaller
Dielectric Losses	higher	lower
Electromechanical Coupling Factors	larger	smaller
Electrical Resistance	very high	lower
Mechanical Quality Factors	low	high
Coercive Field	low	higher
Linearity	poor	better
Polarization / Depolarization	easier	more difficult

The two piezoelectric sensors used for this study have different dimensions but are both rectangular in shape. Piezo-J has dimensions of 2.0x 1.5cm with a thickness of 0.1 cm, *Figure 11*. Piezo-P has two sections the piezoelectric ceramic-with dimensions of 2.3 x 2.0 cm with a thickness of 0.06 cm- and extended area that has thickness of 0.016 cm. The dimensions of Piezo-P are 5.8 x 2.0 cm.

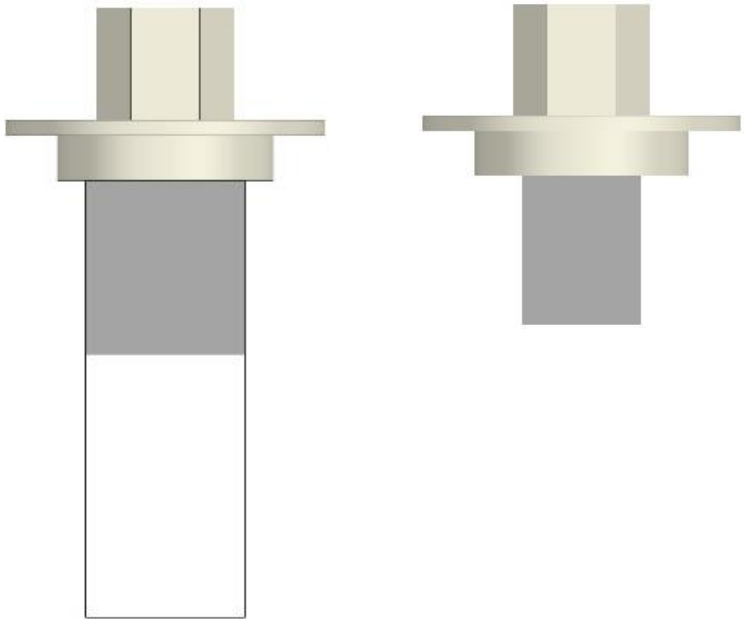

Figure 11 Piezo-P with dimensions of 5.8 x 2 x 0.06 cm and Piezo-J with dimensions 2 x 1.5 x 0.1cm

Both sensors are similar in material composition. The composite materials are a blend of the ceramics with an epoxy or polymer to lower acoustical impedance and produce a higher coupling coefficient. Table 3 summarized the properties of the piezoelectric material that is used. The piezoelectric elements are connected to an oscilloscope channel in order to capture data. The piezoelectric effect results from the linear electromechanical interaction between the mechanical and electrical states in crystalline materials with no inversion symmetry. This study experimentally investigates the relationship between the flow parameters and the voltage signal generated by the sensor.

2.2.6.1.Material Properties of Piezoelectric

Table 3 Material Properties of Piezoelectric

PROPERTY	Units	Symbol	
Coupling Coefficient	–	K_t	0.45
		K_{31}	0.34
Frequency constant	Hz. m	N_p	2200
		N_t	2070
Piezoelectric constant	$\times 10^{-12}$m/v	N_{31}	1680
		d_{33}	320
		d_{31}	-140
Dielectric Constant	@ 1 kHz	$\varepsilon_{33}^{T}/\varepsilon_0$	1400
Curie Temperature	C°	T_c	320
Density	g/cm^3	ρ	7.9

For this study geometry and surface area will be experimentally and numerically studied. The piezoelectric fan includes its own circuit while the piezoelectric ceramic does not. Two cables wires (positive and negative wires) are connected to the Silver electrodes being on both sides of the piezoelectric ceramic, carefully making sure they are properly connected and not touching each other. Then both sensing elements are connected to the corresponding Oscilloscope channel in order to captured data.

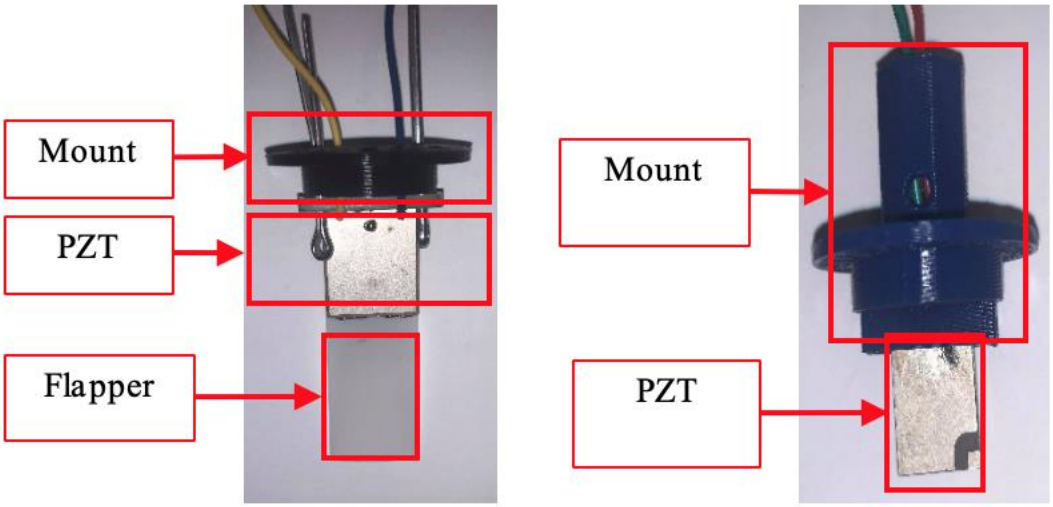

Figure 12 Piezo P and Piezo J with their respective mounting

2.2.7. Test Article Support

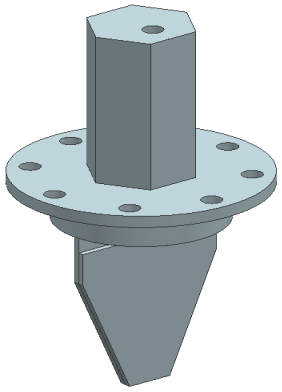

Figure 13 Sensing element and mount

The sensing element mounts are made of PLA. It is designed to be inserted on the top of either the rectangular test or circular test setup and can be rotated 360 degrees relative to the air flow ports. The rotation of the mounting allows for velocity of the air impacting the surface of the sensor at different orientations. However, for this thesis the sensor is always placed perpendicular to the flow. Both mountings are designed according to the specific geometry of the test article. For example: Piezo J is compressed by the mounting in order to hold in place. The handle has

hexagonal cross-section with a though hole for the electrical cable from the ceramic electrodes to be connected to oscilloscope. This was designed to keep the cable management organized, and without disrupting the air flow to hit the face of the ceramic. On the other hand, since Piezo P has a base accessible for mounting. It will be attached to it as shown in figure 13.

2.3. THEORY

The coupled electro-mechanical behavior of piezoelectric materials is defined by two linearized constitutive equations, shown in in Eqs. (1) and (2) (Paufler 1992).

$$\varepsilon_i = S_{ij}^{D}\sigma_j + d_{mi}E_m \tag{1}$$

$$D_m = d_{mi}\sigma_i + \xi_{ik}^{\sigma}E_k \tag{2}$$

Where the indexes refer to different directions within the material coordinate system, σ is the stress vector, ε is strain vector, E is the vector of applied electric field, S are the matrix of compliance coefficients, D is vector of electric displacement , ξ is permittivity, d is the matrix of piezoelectric strain constants, and D and E represent measurements taken at constant electric displacement, constant electric field and constant stress. After a piezoelectric transducer is mechanically stressed, the sensor generates a voltage. This phenomenon is governed by the direct piezoelectric effect Eq (1). This property makes piezoelectric transducers suitable for sensing applications. If a sensor is subject to a stress field, assuming the applied electric field is zero, the resulting electrical displacement vector is:

$$\begin{Bmatrix} D_1 \\ D_2 \\ D_3 \end{Bmatrix} = \begin{Bmatrix} 0 & 0 & 0 & 0 & d_{15} & 0 \\ 0 & 0 & 0 & d_{15} & 0 & 0 \\ d_{31} & d_{31} & d_{33} & 0 & 0 & 0 \end{Bmatrix} \begin{Bmatrix} \sigma_1 \\ \sigma_2 \\ \sigma_3 \\ \tau_{23} \\ \tau_{31} \\ \tau_{12} \end{Bmatrix} \tag{3}$$

The generated charge can be determined from Eq. (4).

$$q = \int \int [D_1\ D_2\ D_3] \begin{bmatrix} dA_1 \\ dA_2 \\ dA_3 \end{bmatrix} \quad (4)$$

Where dA_1, dA_2 and dA_3 are the differential electrode areas in the 2-3, 1-3 and 1-2 planes. The generated voltage V_p is related to the charge via Eq. (5):

$$V_p = \frac{q}{C_p} \quad (5)$$

Where C_p is capacitance of the piezoelectric sensor. The piezoelectric effect results from the linear electromechanical interaction between the mechanical and electrical states in crystalline materials with no inversion symmetry. Many forces may impact the stress field. However, based on the experimental setup it is hypothesized that the major contributor to internal stress is the drag force, Eq (6).

$$F_D = \frac{1}{2}\ \rho\ A\ C_D\ v^2 \quad (6)$$

Where F_D is the drag force, ρ is the fluid density of air at room temperature and pressure, A is the surface contact area between the fluid and body, C_D is the drag coefficient, and v is the average velocity of the fluid acting on the surface of the body. The drag coefficient was estimated based on the flow perpendicular to a flat plate ("Shape Effects on Drag," n.d.). The coupling of force and voltage generated in the sensor material is used to determine the velocity of a flow field.

2.4. TEST CONDITIONS

In order to calculate the average velocity acting on the surface of the piezoelectric, the velocity profile inside the test section of the CTS was measured with a hotwire anemometer. The velocity profiles were measured at the same location of the position of the piezoelectric sensor. The velocity profiles within the test section of the CTS were measured at preset settings of States

1 to 4. The velocities associated with these states is presented in *Table 4.* The four different states correspond to different preset values on each experimental setup.

Table 4 Velocities tested in the circular and rectangular test section setups

	Circular Test Section Setup Velocity (m/s)	**Rectangular Test Section Setup Velocity (m/s)**
State 1	1.9	-
State 2	4.3	4.2
State 3	9.0	8.4
State 4	14.5	13.4

Figure 16 presents the velocity profiles at the location of the sensor in the circular cross section setup. The y-axis represents the distance at the centerline of the test section measured in a vertical direction. The test section has a diameter of 10 cm. However, due to the size the of hot wire anemometer the velocity profile near the wall was not measured. At all conditions, the velocity profiles in the CTS were nearly uniform due to the presence of the flow straightener upstream of the test section. At higher velocities, States 3 and 4, the profiles were more strongly influenced by the presence of the wall and no-slip condition as demonstrated by the higher velocity

near the center of the tube. These data were used to calculate the average velocity of the air in contact with the piezoelectric sensor, values shown in table 4.

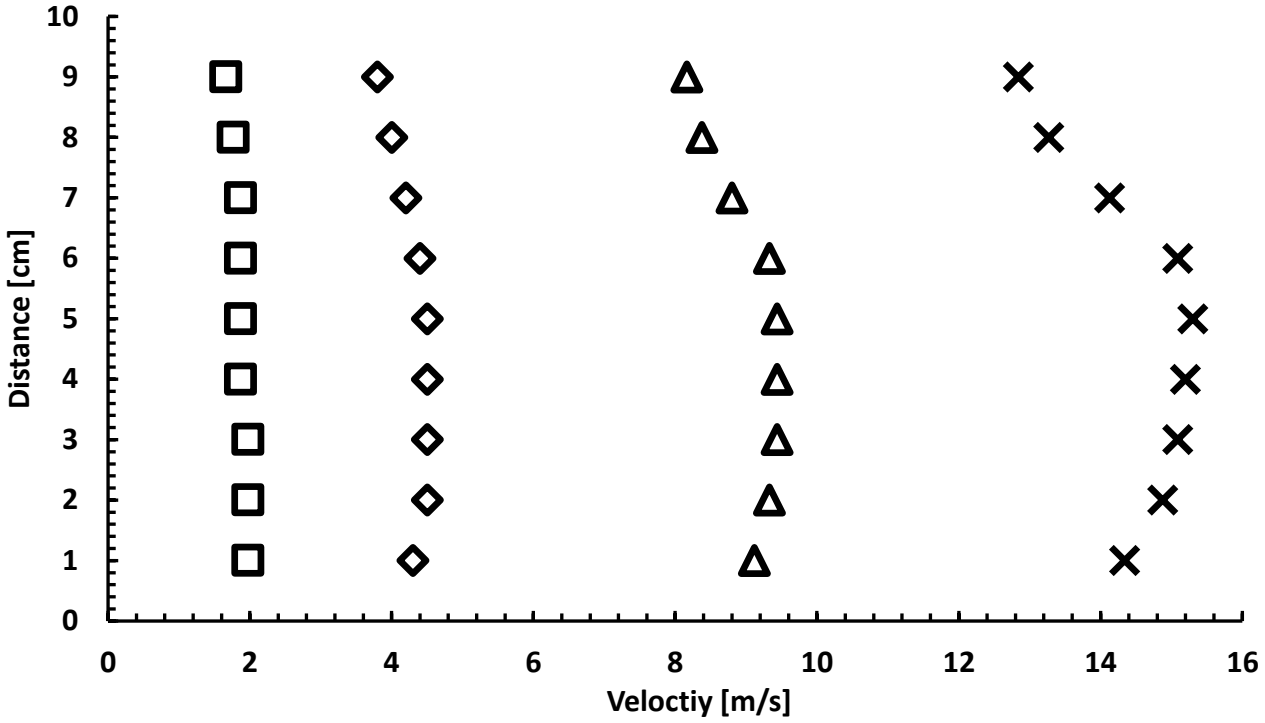

Figure 14 Circular test section velocity profiles: □ = State 1, ■ = State 2, Δ = State 3, and × = State 4

The velocity profiles within the rectangular test section are also measured at preset settings of State 1 to 4. Figure 16 presents the velocity profiles. The test section has height of 8 cm. Near wall velocities were not recorded due to the size the of hot wire anemometer. For these velocity profiles, low velocity is measured near the bottom and top portions of the test section. Due to limitations of the test setup, the system is not able to produce average velocity profiles lower than 4 m/s. After exposure to these profiles, the root mean square (RMS) value of the signal measured from the sensor is then processed using data acquisition software then averaged over the time duration of the test. The measurements were repeated several times and the uncertainties estimated with the student's t-test at 95% confidence level.

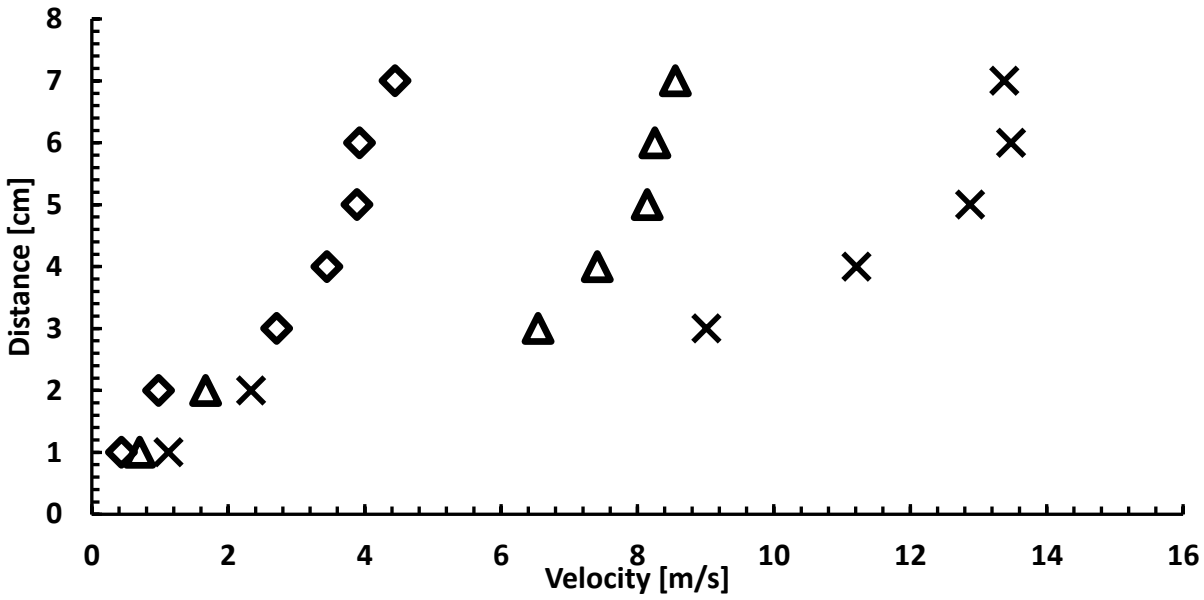

Figure 14 Rectangular test section velocity profile: □ = State 1, ■ = State 2, Δ = State 3, and × = State 4

2.5. STRAIN GAUGE

Due to the sudden expansion from the circular inlet port to the rectangular test section there may be areas of recirculation or flow irregularities not captured by measurement of average velocity. Other potential factors that may contribute to the much higher voltage output of the sensor include material thickness, flexibility, and turbulence levels in the system. With today's emphasis on product liability and energy efficiency, designs must not only be lighter and stronger, but also more thoroughly tested than ever before. (Kamrul Hasan Rahi 2016) The objective of this experiment is to determinate unknown quantities such as strain and stress at given conditions of the piezoelectric sensor. When a body is subjected to a load, the amount of deformation can be expressed as follow:

$$\varepsilon_x = {}^{\sigma_x}/_{E}$$

The Equation above, known as Hooke's law, utilizes Young's modulus of elasticity, E, to create a relation between the stress applied to a body and the strain the body endures. The strain gage is used to the measurement of mechanical quantities. As their name indicates they are used for the measurement of strain. Measurements will be made to obtain the principal stresses and strains on an aluminum cantilevered beam. These measurements allowed us to compare theoretical computations to a physical problem in order to use this as a validation process. In mechanical testing, it is really important to take into account how an object reacts to various forces. Since then a new significance on the subject of experimental stress analysis and the techniques for measuring the amount of deformation a material experiences due to an applied force called strain. The definition is the ratio of the change in length of a material to the original, unaffected length, as shown in Figure 1. Mathematically, it can be shown by:

Figure 15 Strain is the ratio of the change in length of a material to the original, unaffected length ("Measuring Strain with Strain Gages - National Instruments" n.d.).

$$\varepsilon = \frac{\Delta L}{L}$$

The strain of a body is caused by an external or internal effect such as force, pressure, moment, heat, structural change of the material. The strain gage must be mounted on the surface of the specimen of which the stress shall be determined and test its accuracy. This is done with the aid

of special bonding adhesives. A strain gage's electrical resistance varies in proportion to the amount of strain in the device. The metallic strain gage consists of a very fine wire arranged in a grid pattern. The grid pattern maximizes the amount of the metallic wire to strain in the parallel direction. The grid is bonded to a thin backing called the carrier, which is attached directly to the test specimen. Therefore, the strain experienced by the test specimen is transferred directly to the strain gage, which responds with a linear change in electrical resistance.

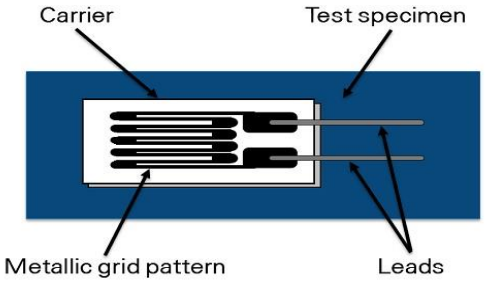

Figure 16 The electrical resistance of metallic grid changes in proportion to the amount of strain experienced by the test specimen.(Fundamentals National Instruments Measurement 2014)

A fundamental parameter of the strain gage is its sensitivity to strain, expressed as the gage factor (GF). GF is the ratio of the fractional change in electrical resistance to the fractional change in length, or strain:

$$GF = \frac{\Delta R/R}{\Delta L/L} = \frac{\Delta R/R}{\varepsilon}$$

The GF for metallic strain gages is around 2 and the particular strain gauge used had a resistance of 120 ohm as stated from the sensor documentation.

Table 5 Strain Gauge specifications

Product Specifications	Attribute Value
Dimensions	9.5 x 3.5 mm
Maximum Operating Temperature	+80 °C
Minimum Operating Temperature	-30 °C
Terminal Type	Wire Lead

In practice, the magnitude of measured strain is expressed as microstrain (με), which is ε x 10^{-6}. Although dimensionless because strain is expressed in units such as mm/mm. Therefore, to measure the strain, you have to measure very small changes in resistance. To measure such small changes in resistance, strain gage configurations are based on the concept of a Wheatstone bridge. The general Wheatstone bridge, illustrated in Figure 4, is a network of four resistive arms with an excitation voltage, V_{EX}, that is applied across the bridge.

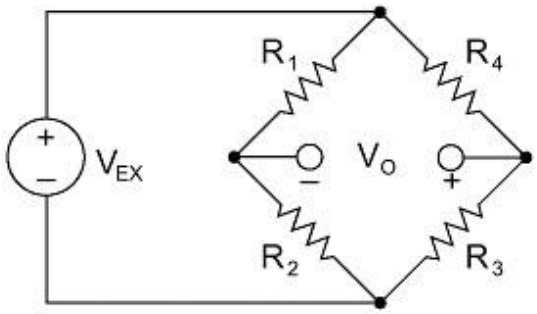

Figure 17 Strain gages are configured in Wheatstone bridge circuits to detect small changes in resistance. (Fundamentals National Instruments Measurement 2014)

The Wheatstone bridge is the electrical equivalent of two parallel voltage divider circuits. R_1 and R_2 compose one voltage divider circuit, and R_4 and R_3 compose the second voltage

divider circuit. The output of a Wheatstone bridge, Vo, is measured between the middle nodes of the two voltage dividers.

$$V_O = \left[\frac{R_3}{R_3 - R_4} - \frac{R_2}{R_1 + 2}\right] V_{Ex}$$

When $R_1 / R_2 = R_4 / R_3$, the voltage output V_O is zero. Under these conditions, the bridge is said to be balanced. Any change in resistance in any arm of the bridge results in a nonzero output voltage. Therefore, if R_4 is replace in Figure 18 with an active strain gage, any changes in the strain gage resistance unbalance the bridge and produce a nonzero output voltage that is a function of strain.

The four different types of strain are axial, bending, shear, and torsional. On this case, bending strain measures a stretch on one side of a material and the contraction on the opposite side due to the linear force applied in the vertical direction.

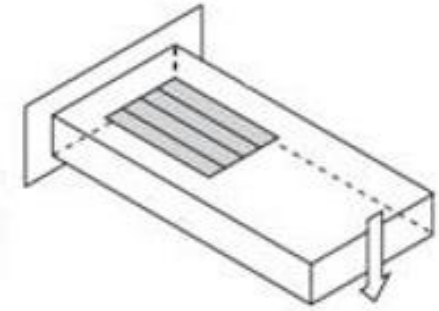

Figure 18 Bending strain measures a stretch on one side and a contraction on the other side

The three types of strain gage configurations, quarter-, half-, and full-bridge, are determined by the number of active elements in the Wheatstone bridge, the orientation of the

strain gages, and the type of strain being measured. The strain gage is connected to a cantilever beam whose lead wires are configured in a half Wheatstone bridge configuration.

2.5.1. Strain Gage Installation

Installing strain gages can take a significant amount of time and resources, and all depends on the bridge configuration. The number of active gages, number of wires, and mounting location can affect the level of complexity required for installation. The strain gauge is bonded to the test specimen with Loctite 401 to one side of a beam Figure 22. If the cantilever beam is bent, the strain gauge will be stretched, increasing resistance. Same procedure is applied when the strain gage is applied to both piezoelectric sensors.

Figure 19 Strain gauge attached to a cantilever beam

Ni LabVIEW NXG, a user interface program, is used to interpret changes in wire resistance on the strain gage into a numerical value, in microStrains. The NI 9237 bridge module used with CompactDAQ 9174 and NI 9923 accessory contains all the signal conditioning

requirements to power and measure the strain gage. The NI-9237 has 10 pins for one out of the four channels. These pins correspond to:

Table 6 NI-9237 pinout for each channel

Pin 1	SC	Shunt Resistor end 1
Pin 2	AI+	Channel Input +
Pin 3	AI-	Channel Input -
Pin 4	RS+	Remote Sense +
Pin 5	RS-	Remote Sense -
Pin 6	EX+	Excitation +
Pin 7	EX-	Excitation -
Pin 8	T+	TEDS+
Pin 9	T-	TEDS-
Pin 10	SC	Shunt Resistor end 2

The NI-9237's internal bridge completion resistors. EX+, EX-, and AI+ still need to be connected by the user. Quarter Bridge II configuration is connected to the NI-9237 as if it were a Half Bridge. R4 is the active quarter bridge strain gage. R3 is a dummy resistor placed perpendicular to the direction of strain and will therefore exhibit changes in resistance only due to temperature drift.

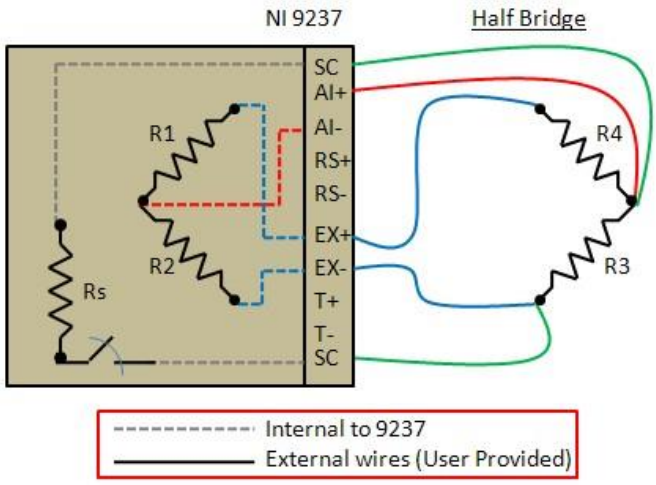

Figure 20 Half bridge configuration using NI 9237 module

Chapter 3: Results and Discussion

3.1. Effect of Area on Piezoelectric Voltage

This section presents results for the piezoelectric sensors placed in the circular test section setup. The two piezoelectric sensors tested were Piezo-P a piezoelectric fan blade with a resonant frequency of 50 Hz and Piezo-J a piezo ceramic plate and were acquired through the company Steminc. Both produced different output voltages for the same flow rates. The following graph shows the resulting signal generated by Piezo-P where each point represents the average RMS value. State 0 is measured when the fan was off and there is no air flowing. The trend of the data show that as the flow rate increases, the signal output voltage from the piezoelectric increases. The

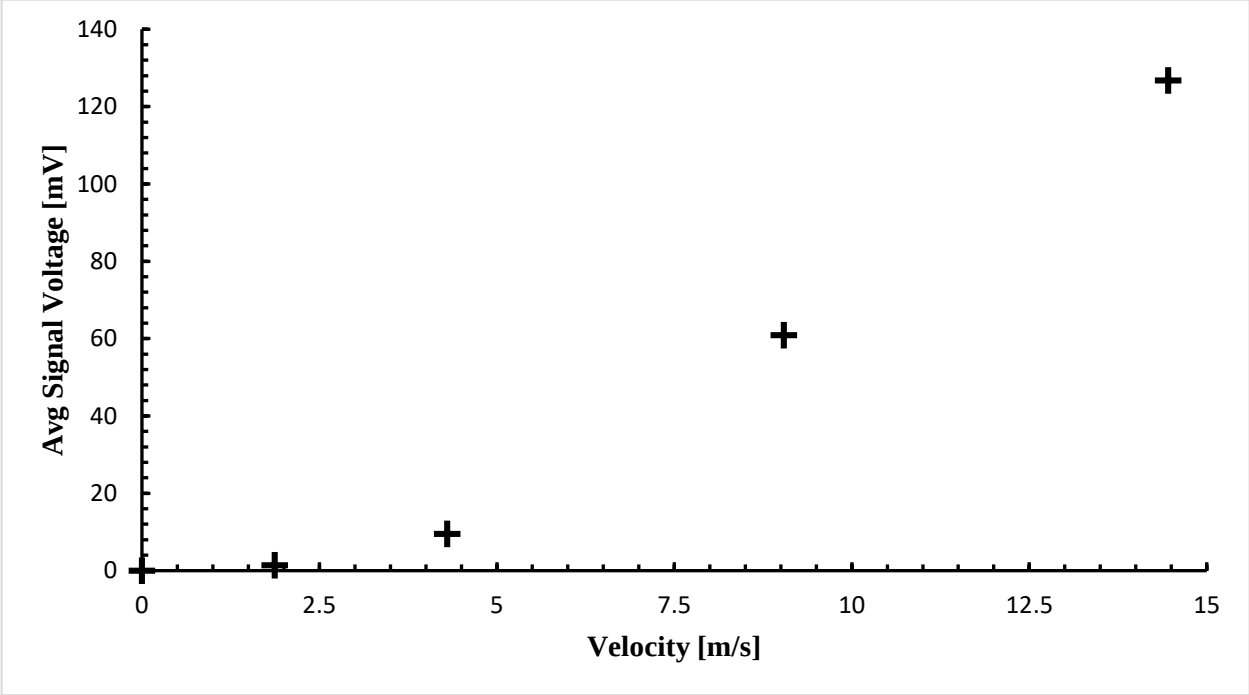

Figure 21 Piezo-P output voltage at the different tested velocities in the circular test section set-up

trend of the increase in voltage is non-linear and reaches the highest voltage at the corresponding highest velocity. The highest voltage measured for Piezo-P is 126.7 mV.

Figure 24 shows the resulting signal generated by Piezo-J. Like Piezo-P, the trend of the data shows that output signal is increasing with the increasing air flow. For Piezo J, a significant decrease in the magnitude of voltage produced is seen at the highest velocity tested. Maximum voltage of 28 mV is observed at the test velocity of 13.8 m/s. It is also observed that at the zero velocity that there is a voltage signal measured, corresponding to a bias error in the measurements. This is also observed for measurements with Piezo-P; however, due to the magnitude of the signal for Piezo-J it is more evident.

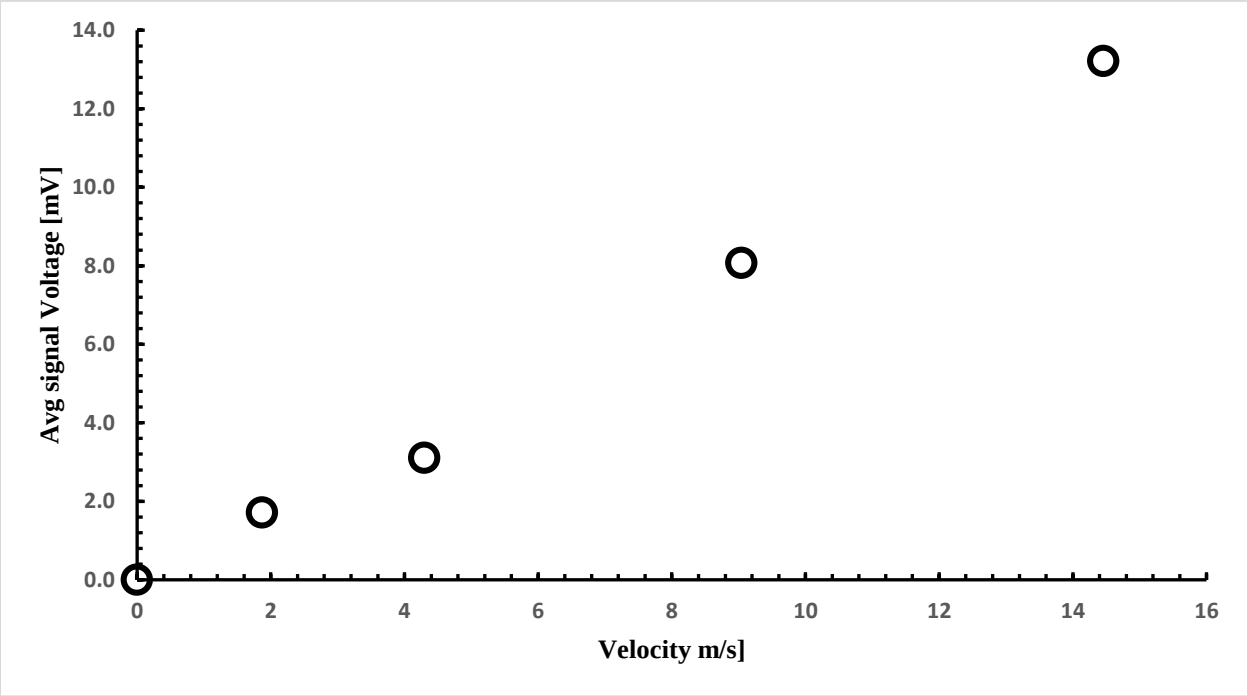

Figure 22 Piezo-J output voltage at the different tested velocities in the circular test section setup

The differences in the output of the two sensors may be attributable to several factors including the contact area, thickness, and drag force acting on the piezoelectric. Contact area for Piezo-P, 11.6 cm^2, is significantly higher than that for Piezo-J, 3 cm^2. In addition, Piezo-P is thinner, 0.06 cm, compared to Piezo-J, 0.1 cm. The thinner piezoelectric is more flexible. The effect of drag is also related to the geometry and average velocity profile seen by the piezoelectric. In order to quantify the drag acting on the sensor, drag is calculated for each piezoelectric. Figure

25 shows the estimated drag force based on the averaged velocities and area of the piezoelectric sensor. The parameters in Eq. (6) remain nearly constant, with velocity varying in a parabolic fashion. Piezo-P reaches a maximum drag force at the highest velocity, this is also observed for Piezo-J. The magnitude of the drag acting on Piezo P is 4.5 times greater than the drag on Piezo J and has a very similar trend than what is observed for the measured velocity and voltage output values. This is due to the nearly 4 times larger area of Piezo-P compared to Piezo-J. Voltage output measured from the piezoelectric sensors at the highest velocity is 4.8 times greater for Piezo-P compared to Piezo-J, which falls within experimental uncertainty of the two measurements. Thus, the drag force accounts for most of the motion and produced voltage from the sensor.

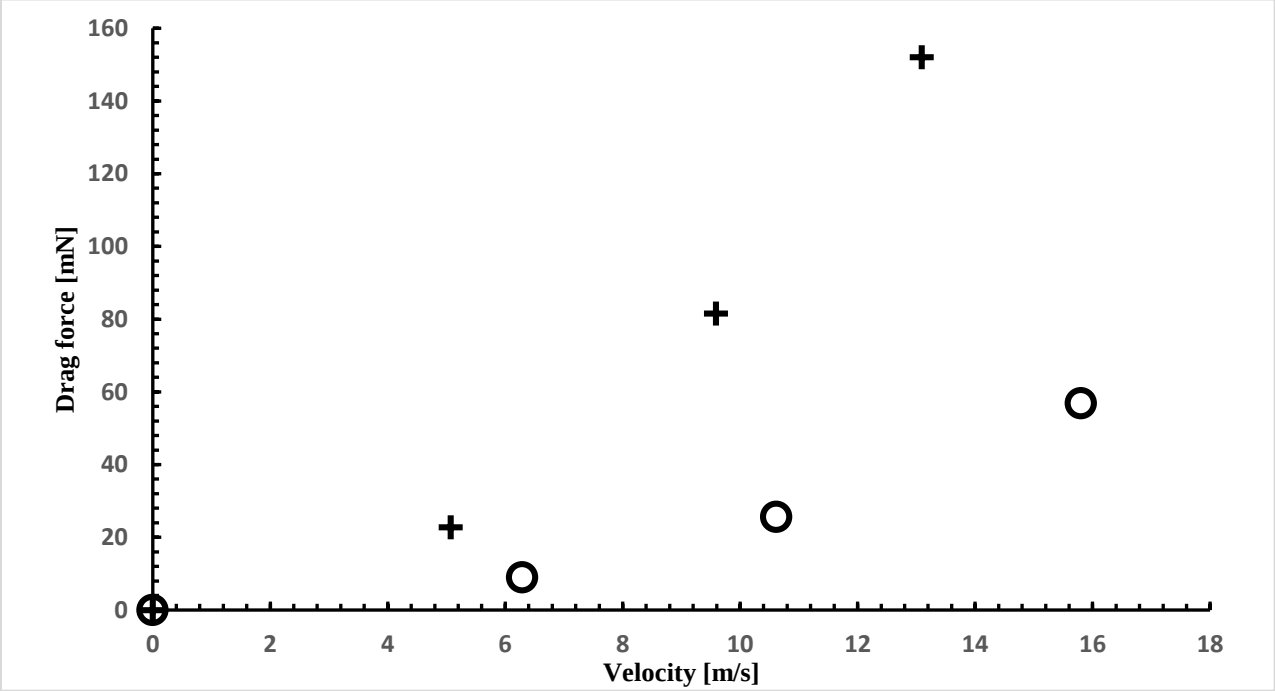

Figure 23 Estimated drag force on Piezo-P (+) and Piezo-J (O) for the different test states (CTS)

Based on these results, it is possible to estimate the flow velocity within a circular cross-sectional test area. The drag acting on the sensor creates a force that results in higher voltage output and accounts for the increase in output. Future experiments will demonstrate that this sensor may also be modified to measure mass flow rate and rapid velocity fluctuations that may occur in the test section.

3.2. Effect of Velocity Profile on Piezoelectric Voltage

This section of the paper investigates the impact of the velocity profile on the voltage output of the sensor. In the previous section a circular cross section with a nearly uniform velocity profile produced a significant increase in voltage for higher tested velocities. In order to test the response of the sensor for a different, less uniform profile, the rectangular cross section testing unit is used. In this section, both piezoelectric sensors are tested in the rectangular test section apparatus. The two piezoelectric sensors produced different output voltages. Figure 25, shows the resulting signal generated by Piezo-P, each point is the RMS value. The trend of the data show that the output signal is increasing when the air flow velocity is increased and reaches the highest voltage at the corresponding highest velocity. The highest voltage is measured for Piezo-P at 370 mV, this is the highest voltage measured for any of the test conditions.

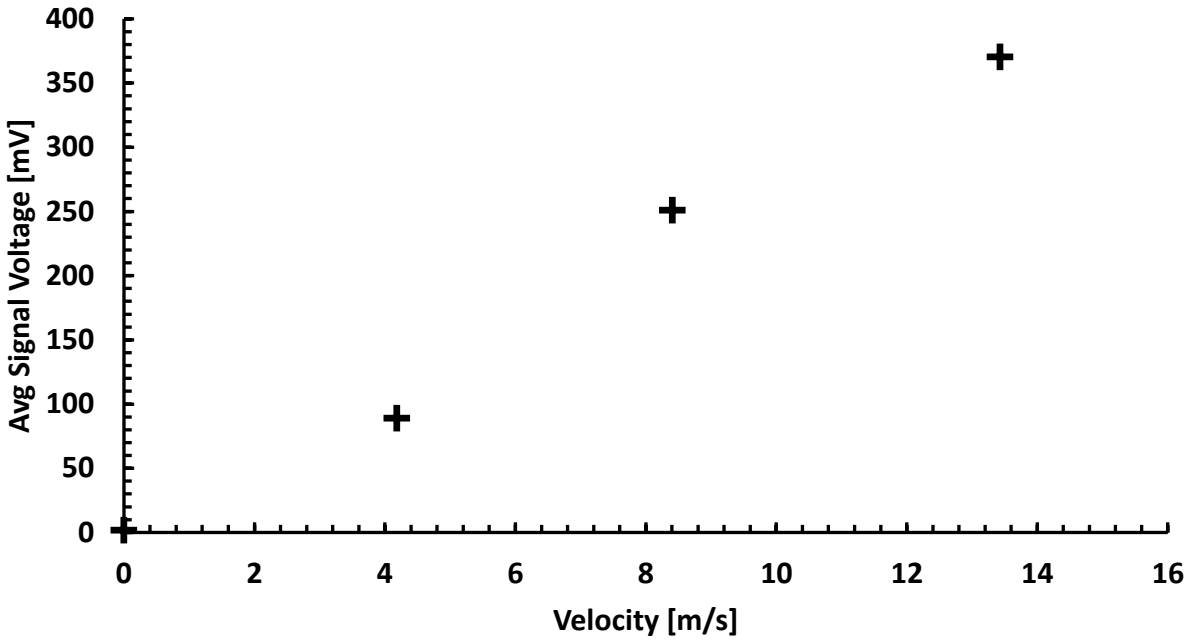

Figure 24 Piezo-P output voltage at the different tested velocities in the rectangular test section setup

Piezo-P produces the highest voltage in the rectangular setup when compared to the circular cross section setup or Piezo-J, Figure 27. The reason for this is that Piezo-P occupies much more of the rectangular test section than the circular cross section and it is more flexible. The velocity of air flow is higher at the center and near zero at the bottom. Piezo-P is exposed to the significantly higher velocities throughout the entire test section. Since the sensor experiences a higher average velocity, it produces significantly higher voltage output. Since Piezo-J is shorter and located closer to the wall and has a larger overall percentage of its area inside of the boundary layer, the voltage output is significantly less than Piezo-P.

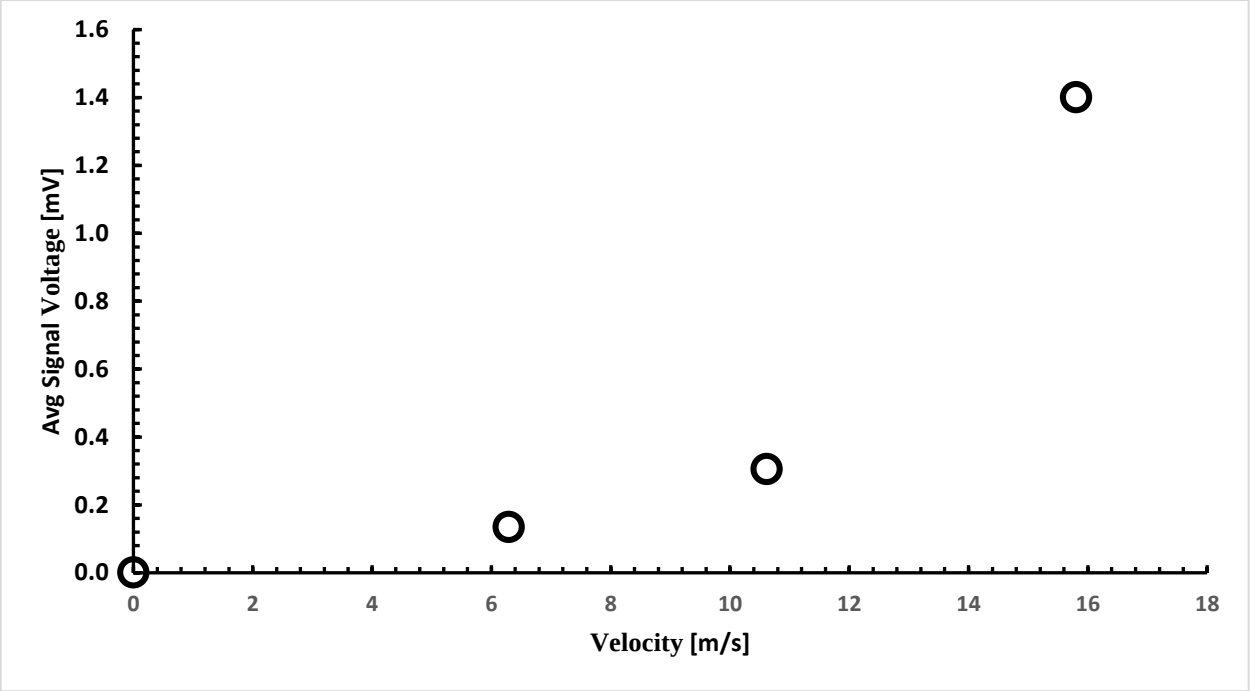

Figure 25 Piezo-J output voltage at the different tested velocities in the rectangular test section setup

In order to estimate the drag acting on the sensor for the different velocity profiles from rectangular test section, drag is calculated for each piezoelectric. Figure 28 shows the estimated drag force. Similar to the results from the CTS, Piezo-P reaches a maximum drag force at the highest velocity, this is also observed for Piezo-J. The magnitude of the drag acting on the larger Piezo-P is 2.7 times greater than the drag on Piezo-J. The magnitude of drag forces acting on Piezo-P in the RTS is smaller by 1.2 times compared to that found from the CTS. In contrast, Piezo-J experiences greater drag force in the RTS by 1.4 times compared to results from the CTS.

Figure 28 shows that Piezo-J produces up to 142.5 times less voltage than Piezo-P at the same conditions. As mentioned previously, this illustrates that the velocity profile exposed to the piezoelectric significantly impacts the voltage output from the sensor. To further illustrate this, Piezo-J produces 11 times less voltage when placed in the rectangular test section setup compared to the circular cross-sectional setup. The same trends for voltage and velocity are observed for

both piezoelectrics, demonstrating the influence of drag force on the sensor. The influence of drag is apparent for the RTS but does not account for the much higher voltage output. In the RTS, the average velocity profiles are presented.

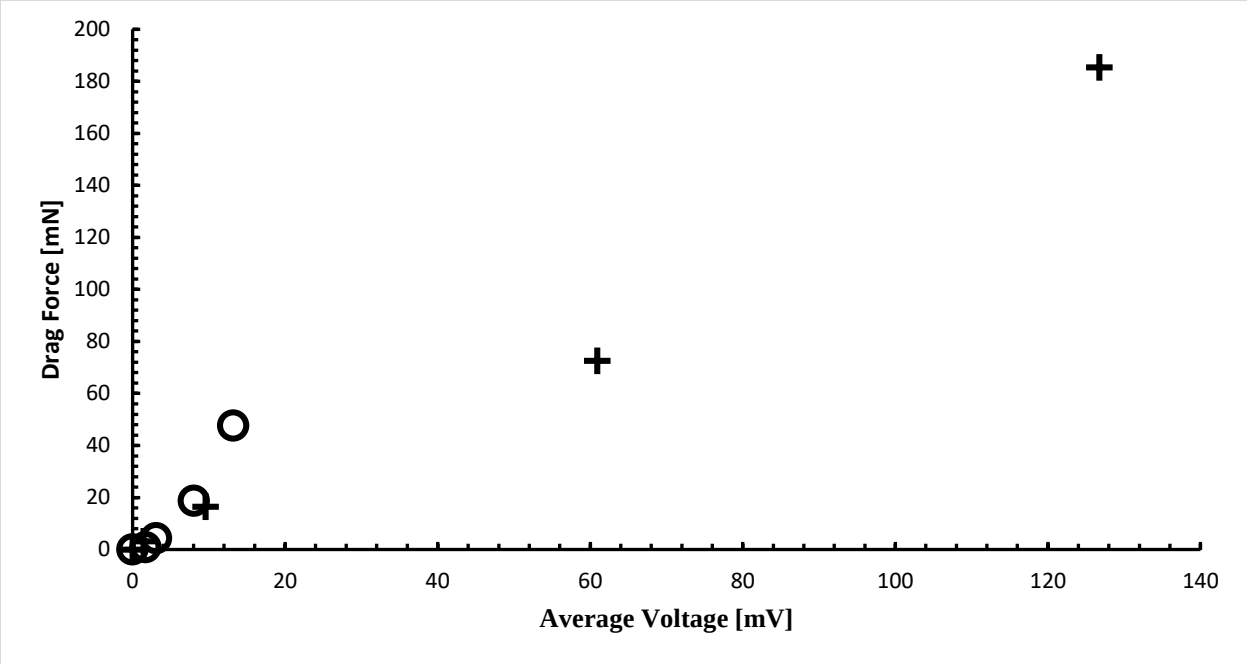

Figure 26 Drag force Vs. Averaged voltage generated on Piezo-P (+) and Piezo-J (o) for the different test states (CTS)

Figure 28 shows the relationship between the calculated drag force acting on Piezo-P and Piezo-J and the voltage generated in the CTS. Both sensors have second order polynomial which fit the prediction from eq (6). Also, Piezo-P has higher drag force due to the higher area and reach 185 mV to respond 126 mN.

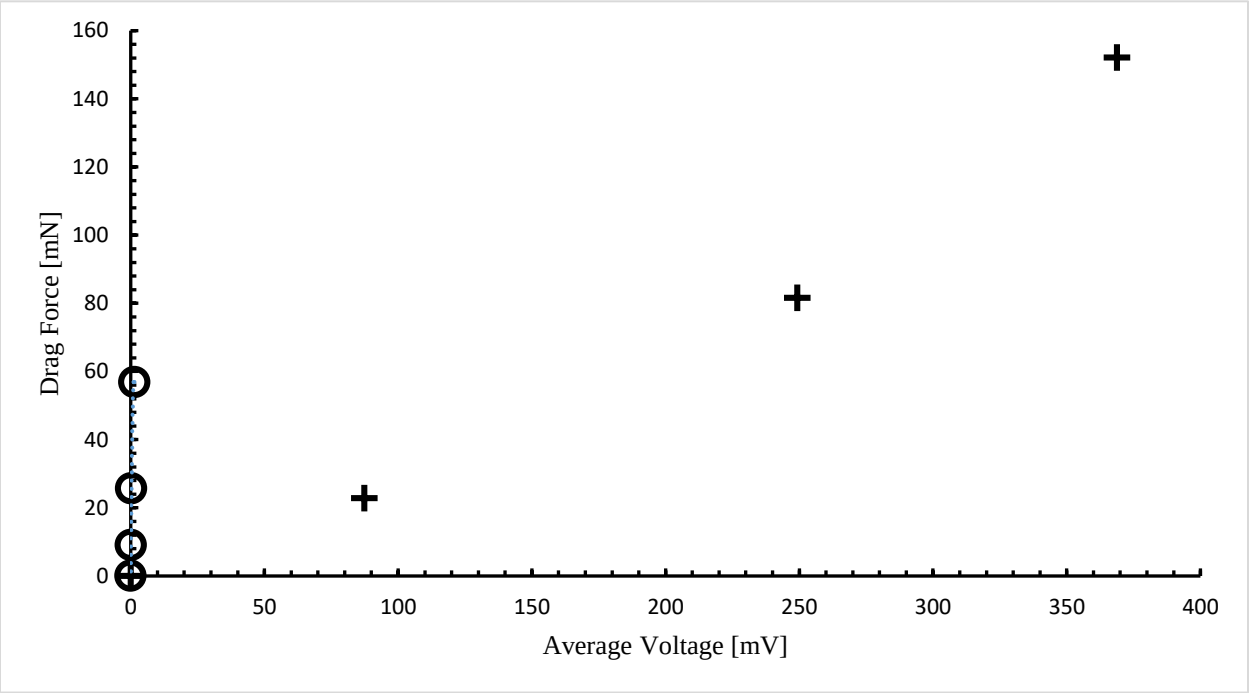

Figure 27 Drag force Vs. Averaged voltage generated on Piezo-P (+) and Piezo-J (-) for the different test states (RTS)

Figure 30 shows the relationship between the calculated drag force acting on Piezo-P and Piezo-J and the voltage generated in the RTS. Both sensors have second order polynomial which fit the prediction from eq (6). Similar to CTS, Piezo-P has higher drag force due to the higher area. The voltage generated from Piezo-J is very small.

3.3. STRAIN MEASUREMENT ON CANTILEVER BEAM

To calculate the microStrains to be expected when loading a cantilever beam with a single load on its free end. The following information is provided:

Material of cantilever beam: Al-6061

Mass used: 50g,70g, 90g, 100g

$$F = ma$$

$$M = FL$$

$$I = {Bh^3}/{12}$$

$$\varepsilon = {Mh}/{2EI}$$

The variables used for equations are: F, force; m, mass; a, acceleration due to gravity; M, moment of force; L, length of beam; I, moment of inertia; b, width of beam; h, thickness of beam; ε, engineering strain; E, modulus of elasticity. All known variables are listed on table 7

Table 7 Known variables on the cantilever beam Al-6061

Known Values	Value	Unit
Modulus of Elasticity, E	6.89E+10	GPa
Mass, m	50, 70, 90, 100	Grams
Acceleration due to Gravity, a	9.81	${m}/{s}$
Length of beam, L	0.06	m
Width of beam, b	0.015	m
Thickness of beam, h	0.000635	m

Using the values and equations provided in previous section, microStrains were calculated for their corresponding applied mass (See table 7). The following graph represent the magnitude of each mass (50g, 70g, 90,g and 100g).

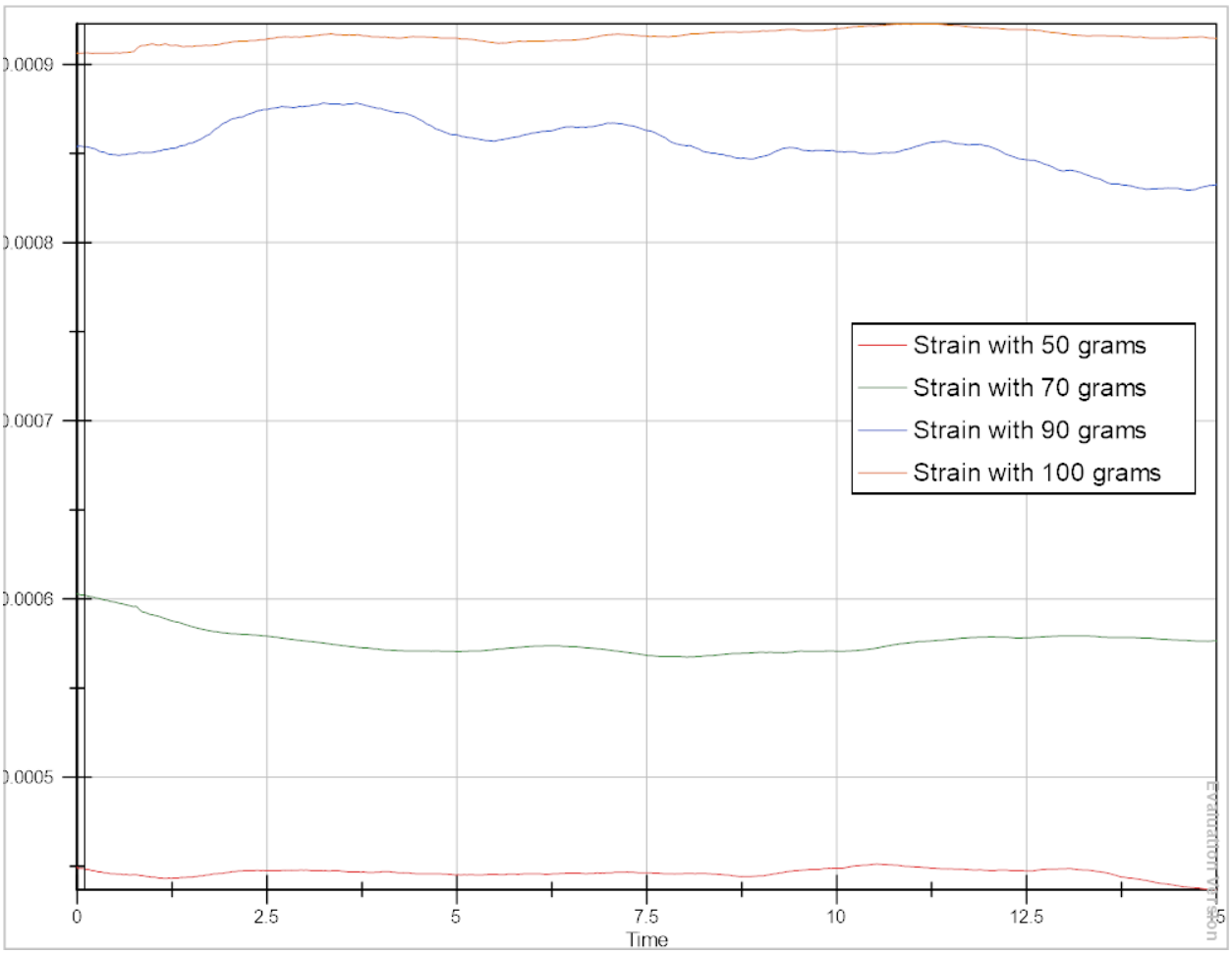

Figure 28 The following graph represent the magnitude of each mass (50g, 70g, 90,g and 100g).

The graph confirmed that the output values correspond to the increasing mas applied on the beam. The below table, along with the graph earlier within this section, conclude that the results are accurate.

Table 8 The table confirmed that the output strain values are similar to the Theorical value microStrain acquired

	Units	Equation	Grams			
			50	70	90	100
Force	N	F=m*a	0.4905	0.6867	0.8829	0.981
Moment	N m	M=F*L	0.02943	0.041202	0.052974	0.05886
Inertia	kg m^2	I=(b*h^3)/12	3.2006E-13	3.2006E-13	3.2006E-13	3.2006E-13
Strain	m/m	e=(M*h)/(2*E*I)	4.23E-04	5.93E-04	7.62E-04	8.47E-04
Theoretical Value micro Strain			423.429	592.801	762.173	846.859
Experimental value micro Strain			446.166	573.740	850.510	917.445
Percentage of Error			-5%	3%	-12%	-8%

This experiment showed a strong comparison between theoretical calculations and the solution obtained through the laboratory procedures. The theorical calculations were used as a starting point to relate the output given by LabView and then validate this method.

3.4. STRAIN MEASUREMENT ON PIEZOELECTRIC SENSORS

After validation, the strain gauge was mounted to both piezoelectric sensors to calculate the strain generated on the sensor inside the circular test section. The final answers represented below are confirmed with Figures # thru #, a LabView output expressing microStrains for a given applied input flow. While running the experiment, data was recorded from LabView onto an excel file. A microStrain vs. time graph can be created.

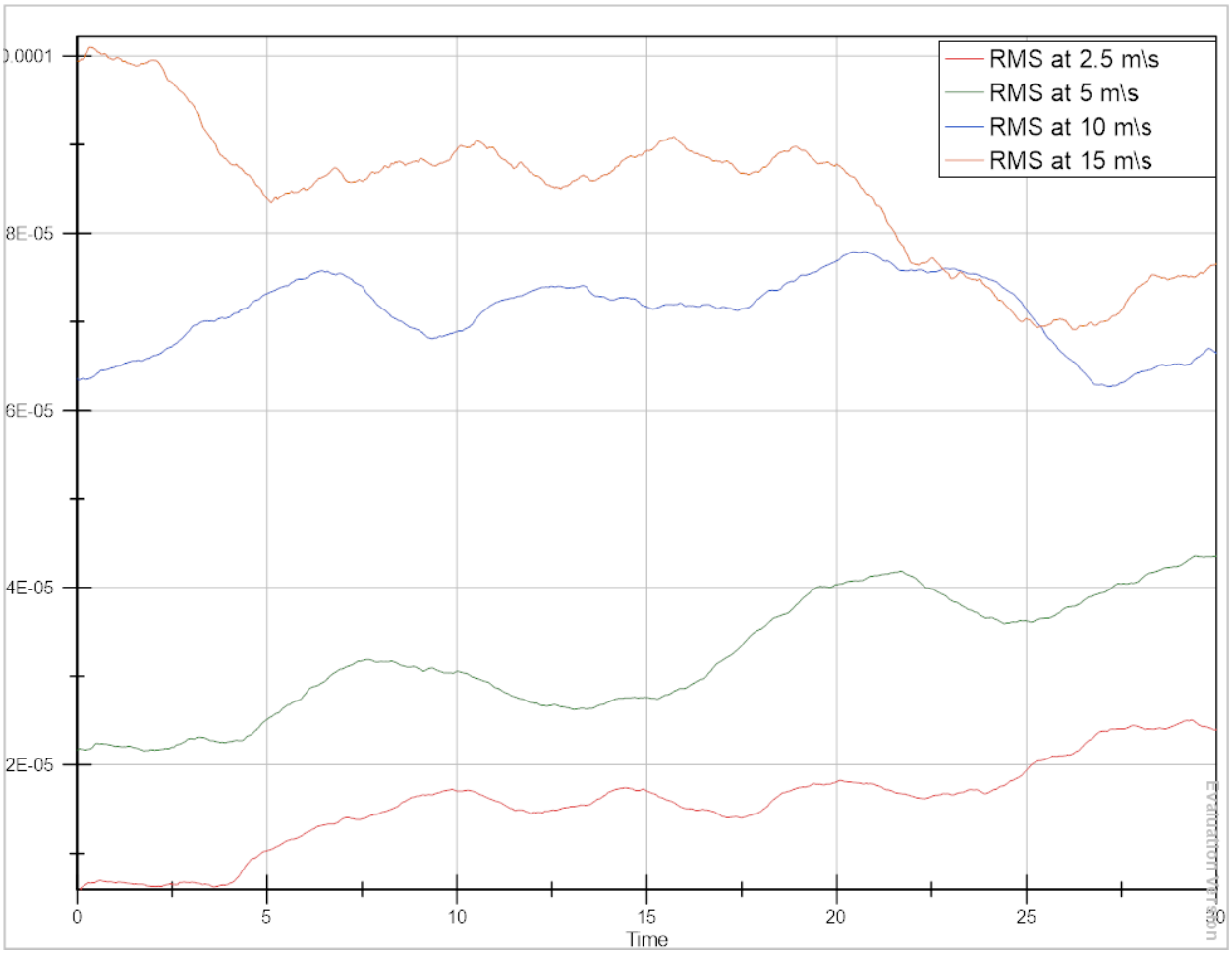

Figure 29 A visual representation of the data collected by introducing a Strain gauge on the CTS set up

The graph below is a visual representation of the data collected. The experiment was constructed and executed multiple times to ensure that the relationship was accurate. The calculations shown in Figure 27 were completed previously to recording data from LabView.

Table 9 The table shows sample data from a test run for the respective input applied

Velocity m/s	Voltage (mV)	Experimental Strain (m/m)	Stress (N/m^2)	Force Single Load (mN)
2.5	1.844	1.63E-05	1.13E+06	66.735
5	9.595	3.29E-05	2.27E+06	134.396
10	61.426	7.13E-05	4.91E+06	291.537
15	127.924	8.50E-05	5.86E+06	347.728

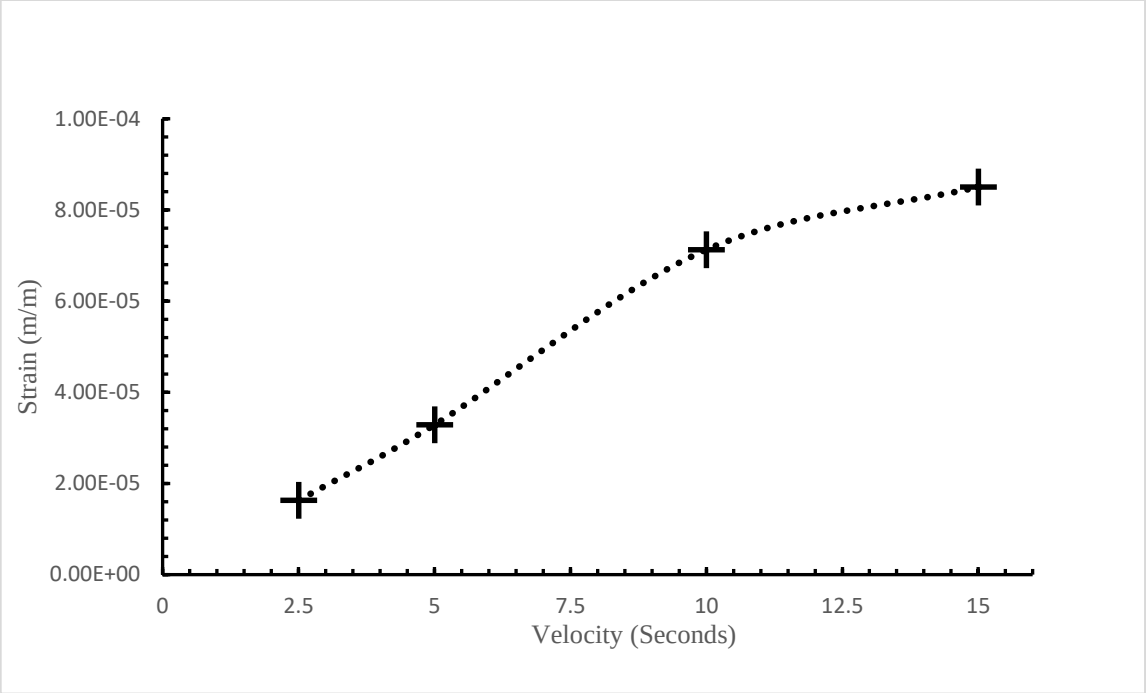

Figure 30The strain generated by Piezo-P in relation to the velocity input on CTS

The strain generated by Piezo-P. The trend of the data shows that as the air flow velocity is increased, the strain output is also increased. The highest strain calculated for Piezo-P at 15 m/s is 8.50x10^ - 5

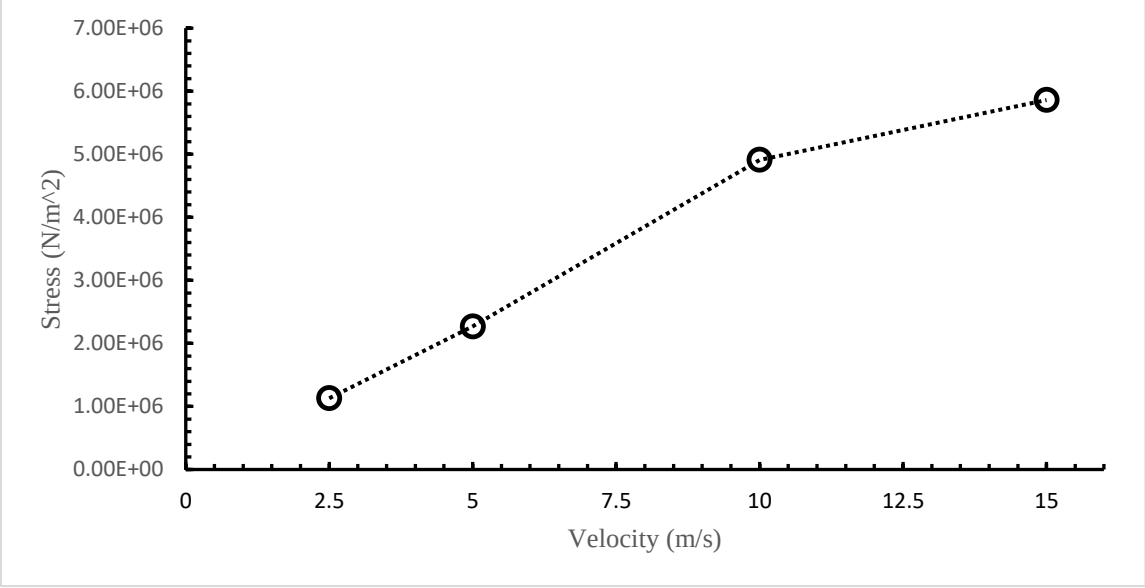

Figure 31 The stress generated by Piezo-P in relation to velocity on CTS

The stress generated by Piezo-P. The trend of the data show that as the air flow velocity is increased, the stress output is also increased. The highest stress calculated for Piezo-P is 5.86x10^6 N/m^6

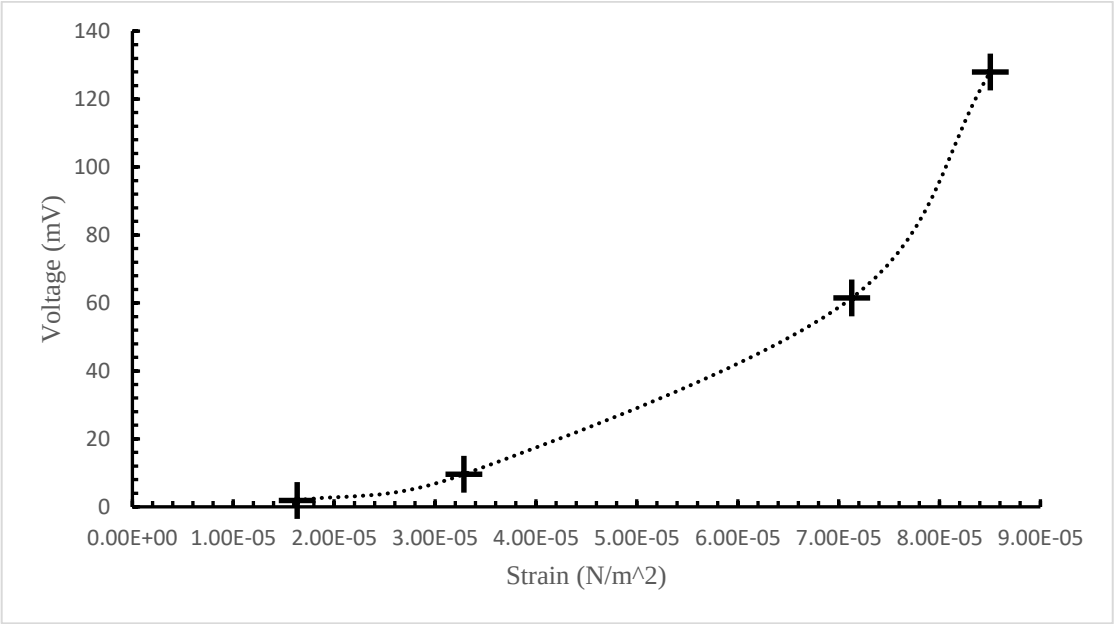

Figure 32 The voltage generated by Piezo-P in relation to the strain

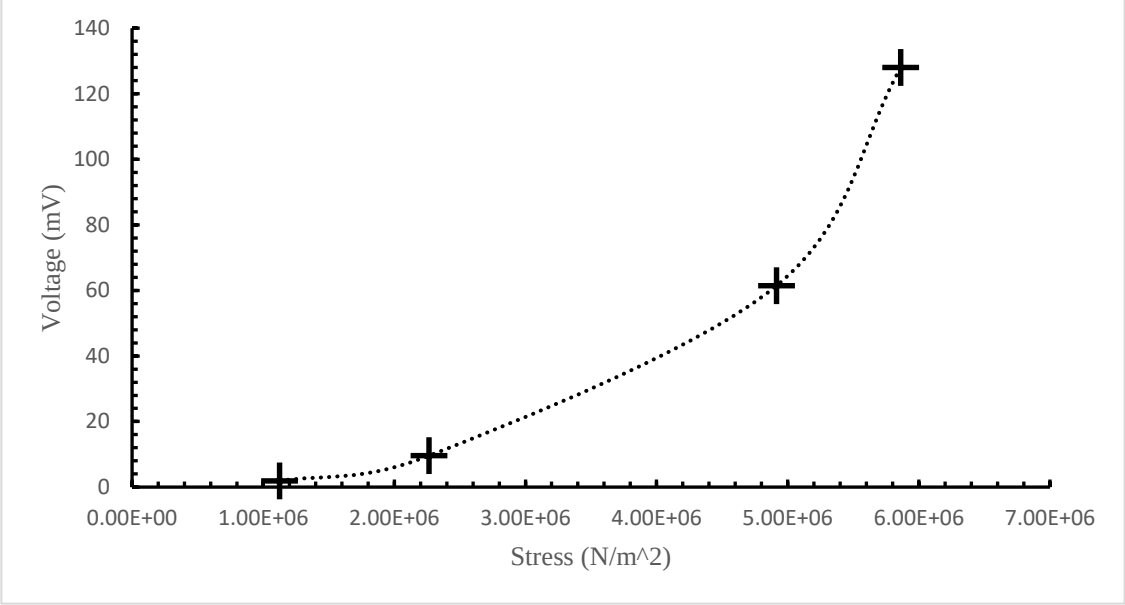

Figure 33 The voltage generated by Piezo-P in relation to the stress

Voltage is related to the strain or strain generated, since piezoelectric characteristics Non-linear increase in strain or voltage.

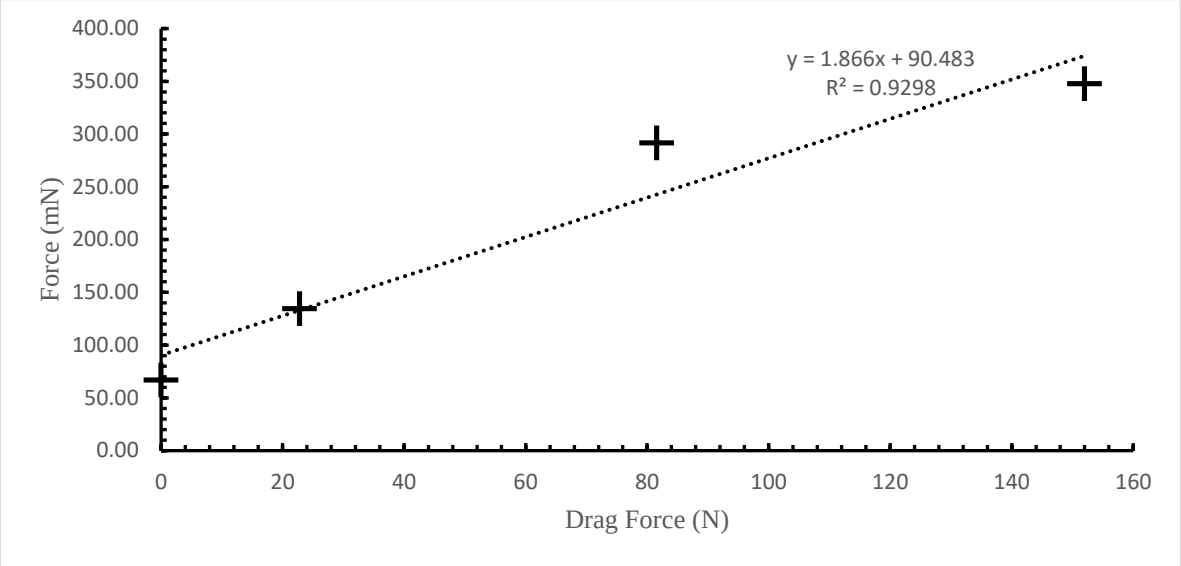

Figure 34 Force Single Load applied on Piezo P with respect to Drag force

Force single load is located at the free end of a sensor. Force Single Load applied on Piezo P with respect to Drag force. This graph demonstrates that not only drag force is a force acting on the sensor inside that system.

Chapter 4: Summary and Future work

4.1. Summary and Conclusions

In many applications in literature, the piezoelectric effect is used in order to produce voltage that is captured for energy harvesting applications. However, in this study the voltage output is used for a different purpose. A piezoelectric cantilever beam is placed in a flow stream and used to measure velocity of a fluid. The piezoelectric is thought to be advantageous due to its fast response time, potential durability at higher temperatures, and self-powered characteristics. The effect of the piezoelectric sensor shape and the influence of velocity profile on the output voltage is presented in this paper. In order to test the impact of piezoelectric shape, two different sized piezoelectrics made of the same material are used. The impact of velocity profile is determined by exposing the piezoelectric to various velocity profiles with two different test sections. The following summarizes the main findings from this study:

- The voltage increases non-linearly as the velocity is increased in the test sections of the experimental setups for both piezoelectrics. This suggests that the piezoelectric voltage output could be calibrated to correspond to different flow velocities.
- The larger piezoelectric, Piezo-P, produces significantly more voltage than the smaller piezoelectric, Piezo-J. Piezo-P has a maximum output voltage 4.8 times higher than Piezo-J when subjected to a uniform flow in the circular test setup. This has been attributed to the increased size of the sensor that causes more drag force. Drag force is calculated to be 4.5 times greater for Piezo-P compared to Piezo-J.
- Due to the non-uniformity of the velocity profiles in the second test setup, Piezo-P produces more than 142.5 times more voltage output compared to Piezo-J. The larger area that

occupies the test section, significantly higher average velocity seen by Piezo-P away from the wall, as well as other factors results in a much higher output signal.

4.2. FUTURE WORK

It is recommended that the strain gauge experiment should use a half bridge with two active strain gauges in the future. The half bridge with both active gauges, in comparison to the one used in this paper, will be more sensitive and able to detect more sensitive strain. With this new half bridge set up, the LabView program must be altered to accommodate. A strain gage cannot measure the stresses directly; it senses the deformations on the surface of structural parts. Since stresses are related to deformations through Hooke's law, results of a strain measurements could be used to predict the stresses generated on both piezoelectric sensors. Then, the piezoelectric sensor will be test at elevated temperatures (200 C) similar temperature that will experience at the Hyper Facility.

References

1. Ambrosio, R., A. Jimenez, J. Mireles, M. Moreno, K. Monfil, and H. Heredia. 2011. "Study of Piezoelectric Energy Harvesting System Based on PZT." In *Integrated Ferroelectrics*. https://doi.org/10.1080/10584587.2011.574989.
2. Čeponis, Andrius, Dalius Mažeika, Genadijus Kulvietis, and Ying Yang. 2018. "Piezoelectric Cantilevers for Energy Harvesting with Irregular Design of the Cross Sections." *Mechanika* 24 (2): 221–31. https://doi.org/10.5755/j01.mech.24.2.18019.
3. Choi, W. J., Y. Jeon, J. H. Jeong, R. Sood, and S. G. Kim. 2006. "Energy Harvesting MEMS Device Based on Thin Film Piezoelectric Cantilevers." In *Journal of Electroceramics*. https://doi.org/10.1007/s10832-006-6287-3.
4. Fundamentals National Instruments Measurement. 2014. "Measuring Strain with Strain Gages." National Instruments Measurement Fundamentals Series. 2014. https://doi.org/10.1109/MCS.2009.935588.
5. "Gas Turbine | Student Energy." n.d. Accessed September 12, 2019. https://www.studentenergy.org/topics/gas-turbine.
6. Hjelmgren, Jan. 2002. *Dynamic Measurement of Pressure - A Literature Survey*.
7. Kamrul Hasan Rahi. 2016. "Design and Construction of a Strain Gauge." 2016. https://www.researchgate.net/publication/321875668_Design_and_Construction_of_a_Strain_Gauge.
8. Kim, Heung Soo, Joo Hyong Kim, and Jaehwan Kim. 2011. "A Review of Piezoelectric Energy Harvesting Based on Vibration." *International Journal of Precision Engineering and Manufacturing* 12 (6): 1129–41. https://doi.org/10.1007/s12541-011-0151-3.
9. Kuchle, J. J., and N. D. Love. 2014. "Self-Powered Wireless Thermoelectric Sensors."

Measurement: Journal of the International Measurement Confederation 47 (1): 26–32. https://doi.org/10.1016/j.measurement.2013.08.041.

10. Li, Qi, Junhua Xing, Dajing Shang, and Yilin Wang. 2019. "A Flow Velocity Measurement Method Based on a PVDF Piezoelectric Sensor." *Sensors (Switzerland)*. https://doi.org/10.3390/s19071657.
11. Liu, Huicong, Songsong Zhang, Ramprakash Kathiresan, Takeshi Kobayashi, and Chengkuo Lee. 2012. "Development of Piezoelectric Microcantilever Flow Sensor with Wind-Driven Energy Harvesting Capability." *Applied Physics Letters* 100 (22): 2010–13. https://doi.org/10.1063/1.4723846.
12. "Measuring Strain with Strain Gages - National Instruments." n.d. Accessed November 25, 2019. https://www.ni.com/es-mx/innovations/white-papers/07/measuring-strain-with-strain-gages.html.
13. Paufler, P. 1992. "Fundamentals of Piezoelectricity." *Zeitschrift Für Kristallographie* 199 (1–2): 158–158. https://doi.org/10.1524/zkri.1992.199.1-2.158.
14. Rosario, Antonio Del. 2004. "Comparison of Energy Systems Using Life Cycle Assessment Officers of the World Energy Council."
15. Sarker, Md Rashedul H., Jorge L. Silva, Mariana Castañeda, Bethany Wilburn, Yirong Lin, and Norman Love. 2018. "Characterization of the Pyroelectric Coefficient of a High-Temperature Sensor." *Journal of Intelligent Material Systems and Structures* 29 (5): 938–43. https://doi.org/10.1177/1045389X17721376.
16. Seo, Young Ho, and Byeong Hee Kim. 2010. "A Self-Resonant Micro Flow Velocity Sensor Based on a Resonant Frequency Shift by Flow-Induced Vibration." *Journal of Micromechanics and Microengineering* 20 (7). https://doi.org/10.1088/0960-

1317/20/7/075024.

17. “Shape Effects on Drag.” n.d.
18. Shen, Dongna, Jung Hyun Park, Jyoti Ajitsaria, Song Yul Choe, Howard C. Wikle, and Dong Joo Kim. 2008. “The Design, Fabrication and Evaluation of a MEMS PZT Cantilever with an Integrated Si Proof Mass for Vibration Energy Harvesting.” *Journal of Micromechanics and Microengineering*. https://doi.org/10.1088/0960-1317/18/5/055017.
19. Sirohi, Jayant, and Rohan Mahadik. 2011. “Harvesting Wind Energy Using a Galloping Piezoelectric Beam.” *Journal of Vibration and Acoustics*. https://doi.org/10.1115/1.4004674.
20. Tucker, David. n.d. “Cooperative Research and Development Agreement (CRADA) Statement of Work (SOW) The University of Texas El Paso and NETL Principal Investigators National Energy Technology Laboratory (NETL).”
21. Tucker, David, Lawrence Shadle, and Nor Farida Harun. 2017. “Automated Compressor Surge Recovery with Cold Air Bypass in Gas Turbine Based Hybrid Systems.” In *International Symposium on Transport Phenomena and Dynamics of Rotating Machinery*.
22. Wang, Yu Hsiang, Chia Yen Lee, and Che Ming Chiang. 2007. “A MEMS-Based Air Flow Sensor with a Free-Standing Microcantilever Structure.” *Sensors* 7 (10): 2389–2401. https://doi.org/10.3390/s7102389.
23. Weinstein, L. A., M. R. Cacan, P. M. So, and P. K. Wright. 2012. “Vortex Shedding Induced Energy Harvesting from Piezoelectric Materials in Heating, Ventilation and Air Conditioning Flows.” *Smart Materials and Structures* 21 (4). https://doi.org/10.1088/0964-1726/21/4/045003.

24. “What Is Piezo-Electric Transducer? - Definition, Piezo-Electric Effect, Theory, Properties & Uses - Circuit Globe.” n.d. Accessed November 26, 2019. https://circuitglobe.com/piezo-electric-transducer.html.
25. Zaccaria, Valentina, David Tucker, Alberto Traverso, and Honolulu Hawaii. n.d. “Cold-Air Bypass Characterization for Fuel Cell Thermal Management in Fuel Cell Turbine Hybrids ISROMAC 2016 International Symposium on Transport Phenomena and Dynamics of Rotating Machinery.”

Appendix

Appendix A: Nomenclature

C_D	Drag Coefficient
F_D	Drag Force
T_c	Curie Temperature C*
V_{EX}	Excitation voltage
V_O	Voltage output
V_p	Generated voltage
ΔL	Change in length
ΔR	Change in resistance
A	Surface contact area
$BaiO_3$	Barium Titanate
Cp	Capacitance
CTS	Circular Test Section
d	Matrix of piezoelectric strain constant
d	Piezoelectric strain constant
DC	Direct current
E	Modulus of Elasticity
E	Vector of applied electric field
F	Force
g	Piezoelectric voltage constant
GF	Gage factor
GT	Gas Turbine
HVAC	Heating Ventilation and air conditioning
K	Electromechancial coupling
N	Frecuency constant
NETL	National Energy Technology Laboratory
NI	National Instruments
PLA	Polylacride
PVDF	Polyvinylidene Fluoride
PWM	Pulse Width Modulation
PZT	Lead Zirconate Titanite
q	Generated charge
QM	Mechanical quality factor
RPM	Revolution per Minute
RTS	Rectangular Test Section
S	Matrix of piezoelectric strain constants
SOFC	Solid Oxide Fuel Cell
v	Average Velocity
Z	Acoustic Impedance
ε	Strain Vector
ξ	Permittivity
ρ	Density g/cm^3
σ	Stress vector

Appendix B: Test Procedure

Setup connectivity

Ensure the physical configuration follows the diagram Figure 10 (System fluid schematic)

1. First of all, connect all equipment following the test procedure instructions and then set parameters before testing. Also follow the safety rules that describe the use of Safety glasses inside the lab and gloves for manipulating the sensor
2. Following the Schematic diagram on chapter two, a 4-WIRE fan has power, ground, and tach signal, and a PWM input. Red wire (power) will be directly connected to red port on power supplier. Blue wire (ground) to black port on power supplier.
3. All three devices are connected to ground and connected to the negative wire from the fan, which is then connected to the black output from the power supplier as showed. Power supplier used an Alligator Clip and Stacking Banana Plug for both ports
4. Fan's positive wire is connected directly to positive output from power supplier
5. PWM wire is connected to the function generator output in order to control the duty cycles using a Test Lead BNC Male to Test Clips wire
6. On this case, Tachometer wire is connected to the first channel on the oscilloscope using the Scope Clip Oscilloscope Probe cable
7. Two cables wires (positive and negative wires) are connected to the piezoelectric ceramic, carefully making sure they are properly connected and not touching each other. Then they are connected to the corresponding Oscilloscope channel in order to captured data. Cables used were a cable BNC Male to BNC Male cable and a BNC Male cable to Test Clips wire. On the case of the piezoelectric fan which has cables

attached to it, just connected the corresponding wires to the sensor and insert it to channel to process data

8. Looking for the velocity profile, the anemometer and hotwire are portable devices and does not require any connections. They are be placed at the same spot as the sensing element for velocity measurements.

Function generator

Function generator is set to a square wave function Six blue buttons allow you to select the following parameters of the output waveform to control fan's duty cycles. After selecting a parameter, the parameter value can be adjusted with the numbered keys, arrow buttons, and the knob located in the upper- right corner of the front panel. The highlighted label corresponds to the parameter that is currently selected, and its value will be shown on the display. You will only need to adjust the Freq, Amplitude, Offset, Width, and/or Duty Cycle parameters.

Table 10 Function generator parameters

Parameters	**Value**	**Units**
Frequency	2	kHz
Amplitude	2.5	V
Offset	1.25	V
High level	2.5	V
Low level	0	V

Amplitude and Offset softkeys toggle together, to Hi-Level and Lo-Level, respectively. Output button turns on the output voltage, which should be off to have a 100% duty cycle

Power supply

Power supplier is set to a nominal voltage of 24 V

DC Axial fan

After the fan turn on, it must be warmed up for 5 min to reach a steady state

Oscilloscope configuration

A storage oscilloscope can capture a single event and display it continuously, so the user can observe events that would otherwise appear too briefly to see directly

- To operate an oscilloscope, you first plug the electrical signal you'd like to view into one of the oscilloscope's inputs (channel one)
- Digital Oscilloscope is set to auto to display automatic calculations for the most efficient display adjustment (changes will be made for different purposes)
- Click back on menu in order to close Auto settings
- Click on CH1 (channel one) and set Coupling to DC, Bandwidth limit to "ON" status, Probe x1, and digital filter must be off
- The vertical deflection is set to 100 mV
- The horizontal sweep is set to 10 seconds
- An oscilloscope's trigger function is important to achieve clear signal characterization, as it synchronizes the horizontal sweep of the oscilloscope to the proper point of the signal. The trigger will be adjusted to stabilize repetitive waveforms as well as capture single-shot waveform. Trigger is set to the 50% button which sets the trigger level to the center of the signal
- Under common menu bottoms click on Acquire and make sure, Acquisition is set to normal, sampling is on real time, memory depth set to long memory, and finally sinx/x is 'ON'

Testing

- During testing, all equipment should be on a table with no movement at all since it could affect lectures on the oscilloscope
- After all parameters are set and check, modified the necessary duty cycle for testing
- For multiple testing, **30 seconds** is enough between each test to let the flow stabilize before importing data
- A full duty cycle test consists on (20,30,40,50,60,70,80,100, and 20 %) and (2.5,5,10, and 15 m/s)

Post-test

- Connect a USB Flash Drive to the USB Host of the oscilloscope
- Press “Storage” button and a menu appears on the right side of the screen
- Press the “Storage” button to select “Bit map” or ‘’ CSV’’. These files can be saved and opened directly in Excel or other PC-based analysis tools.
- Data depth should be on maximum and Para Save set ‘ON’ to save the current oscilloscope settings in different format with the same file name
- Press “External” button and a new menu appears on the screen.
- Press “New File” button and a new menu appears on the screen. Use Multi-function knob on the oscilloscope to name the file and press “Ok” to save the file to the USB Flash Drive as a bit map file or csv file. Saving to external USB may take some time.

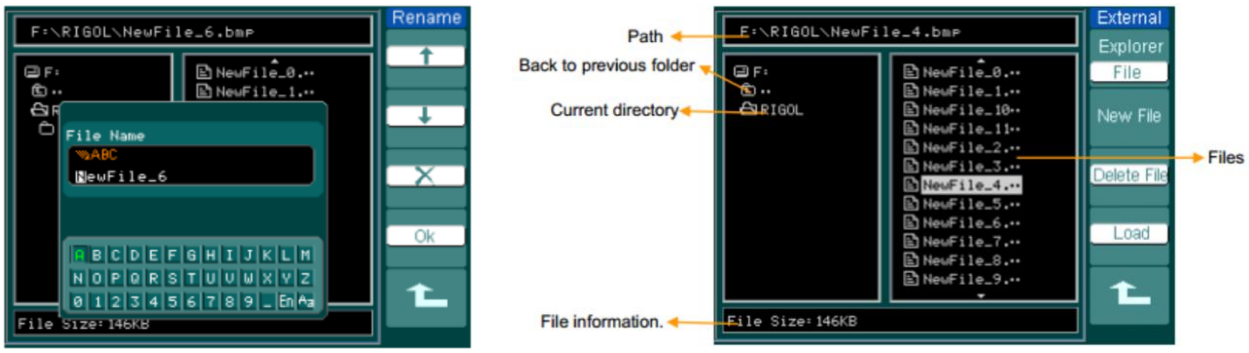

Figure 35 Saving data from oscilloscope

Appendix C: Safety Considerations

Personal protective equipment (PPE) will be used at all times and for the following phases of the experiments: Test Setup Buildup, Hardware Installation, and general test operations.

Table 11 Personal Protective Equipment

Eyes	Safety glasses shall be worn at all times when inside the lab
Feet	Closed toe shoes (steel toe) shall be worn at all times when inside the lab
Body	Lab coats shall be worn at all times inside the lab
Ears	Ear protection shall be worn by technicians inside bunker when loud noise is occurred at the lab (above 15 dB)

Appendix D: Hazard Analysis

LEAD ZIRCONATE TITANATE (PZT) PIEZO CERAMIC

IDENTIFICATION:

Product type: Lead Zirconate Titanate (PZT)

Chemical Family: Ceramic Materials

Formula: Proprietary

Table 12 PZT Hazardous material percentage

Hazardous Components	**Material %**
Lead Oxide	55-72
Zirconium Oxide	4-25
Titanium Oxide	4-15

PHYSICAL DATA:

Form: Solid Ceramic Material

Appearance: Yellow – White - Silver

Odor: None

Solubility in Water: Insoluble

Hazards/Reactivity:

Instability: This product is normally stable

Incompatibility: None

Polymerization: This product does not normally polymerize significantly

Fire & Explosion Data:

Flash Point: None; solid material

Fire & Explosion Hazards: None, nonflammable

Health Hazard Information:

Solid Lead Zirconate Titanate (PZT) ceramic materials are generally non-hazardous but toxic dust may be generated by breaking it or machining processes. The primary route of entry is either by inhalation or ingestion. This material can be in the form of a powder or solid. If inhaled or ingested the toxicology of lead predominates. This includes the potential for damage to the kidneys, blood forming organs as well as the reproductive system and the nervous system. Ingestion can cause vomiting, diarrhea, nausea and abdominal pain. Inhalation may cause irritation of the nose and throat, cough, dyspnea, chest pains, fever and chills. PZT ceramics contain Lead which is a known carcinogen.

Material Safety Data Sheet (MSDS) Piezoceramic Material

Acute lead poisoning can lead to a condition called acute encephalopathy, which may rapidly develop into seizures, coma and eventually death.

Exposure Limits:

Table 13 PZT exposure limits

Material Name	OSHA PEL (mg/m3)	ACGIH TLV (mg/m3)
Lead	0.05	0.05

Zirconium Oxide	5.0	5.0
Titanium Oxide	15.0 (Total dust)	10

First Aid Instructions:

Ingestion: If conscious, induce vomiting.

Inhalation: Remove to fresh air and if breathing is difficult give oxygen.

Skin Contact: Wash thoroughly.

Eye Contact: Flush with plenty of water for 15 minutes.

In all cases seek appropriate medical advice & treatment.

Personal Protection Information:

Respiratory Protection: Selection of a suitable respirator will depend on the properties of the contaminant(s) and their actual or expected air concentration(s) versus applicable limits. Gloves: Gloves should be used when the possibility of skin contact exists. The suitability of a particular glove and glove material should be determined as part of an overall glove personal protection program. Considerations should include chemical breakthrough time, permeation rate; abrasion, cut and puncture resistance; and duration of contact, etc. Recommended glove material: Latex.

Other personal protection practices: Appropriate eye protection such as safety glasses should be used where the possibility of eye contact exists. Protective outer clothing should be used where the possibility of body contact exists. Contaminated work clothing should not be allowed out of the workplace. Smoking or the consumption of food or beverages should be prohibited where the material is handled or stored. After handling this material wash hands thoroughly before leaving

the work area.

Additional Engineering Controls: Local exhaust ventilation is recommended where an airborne dust or powder is generated. Work practices and training may be required depending on the exposure level. Many of these points are discussed in the OSHA Respiratory Protection Standard (29 CFR 1910.134), the OSHA Hazard Communication Standard (29 CFR 1910.1200) and the OSHA Lead Standard (29 CFR 910.1025).

Disposal Information:

Contaminated items: Empty product containers, contaminated clothing and cleaning materials, etc. should be considered hazardous until decontaminated or properly disposed of. Dispose of waste in accordance with federal, state and local regulations. Typically defined as a hazardous waste by EPA.

Storage Information:

Store in tightly closed containers. Label with name of contents.

Fan's Safety Regulations

Pay attention to the following warnings to avoid risk to persons or malfunctioning. The following risk ratings are used in this operating manual to denote potential risk situations and important safety instructions:

Hazard classification of warning notices	**DANGER**	**WARNING**	**CAUTION**	**SOLUTION**
Basic safety regulations	N/A	Impermissible high load	N/A	Stop the product immediately after impermissible loading (e.g. impact, heat, overvoltage).

Electrical voltage and current	Electrical voltage	N/A	N/A	Regularly check the electrical equipment of the product. Eliminate immediately loose connections and defective cables.
			Electrical voltage	Only connect the product to current circuits that can be switched off by a switch (all poles disconnected). When working on the product, secure the system/machine in which the product is installed against switching on again
	Electrical voltage at motor	N/A	N/A	Wait five minutes after the voltage (all poles) has been switched off before opening the product
Safety and protective functions	Missing safety device and faulty protective equipment.	N/A	N/A	Without protective equipment severe injuries can occur, e.g. by taking hold of the rotating equipment. Operate the product with protection guards only.
	Electromagnetic radiation	N/A	N/A	Electromagnetic compatibility (EMC) may affect the system integration of the product due to interaction. Ensure the electromagnetic compatibility of the entire system.
Moving parts	DANGER Self-starting product	N/A	N/A	If voltage is applied, the motor automatically restarts after a mains failure or when blocking has been eliminated. Do not stand in the danger zone of the product. Switch off the mains voltage when working on the product and secure against switching on again.
	DANGER Rotating impeller	N/A	N/A	Contact with the impeller may result in injuries. Before starting the product, ensure that it is securely fixed and that the guards are in place.
		N/A	High risk of fire spreading	High risk of fire spreading. Can cause fire to spread. Never direct the airflow (intake/exhaust side) at a potential source of fire.
	Blocking of escape routes	N/A	N/A	The product can create dangerously high pressure. When operating the product ensure that there is adequate supply and exhaust air.
	N/A	Parts transported by the airflow	N/A	The product can transport small parts in the airflow and catapult them out. Ensure that there are no loose small-

				parts in the intake and exhaust area. Do not stand in the danger zone of the product.
	N/A	Rotating fan	N/A	Long hair, loose-fitting garments and jewellery can be caught and pulled into the product. Risk of injury. Do not wear loose-fitting garments or jewellery when working on moving parts. Protect long hair by wearing a hair net.
Hot surface		N/A	High temperature at motor housing. Risk of burns	Hazard classification of warning notices
Emissions	Acoustic alarms can be overheard.	N/A	N/A	Alarm signals can be overheard. Take technical protective measures, e.g. optical warnings.
	N/A	A noise pressure level higher than 70dB(A) is possible depending on the installation and operating conditions.	N/A	Risk of deafness due to noise. Take technical protective measures. Provide operating personnel with protective equipment, e.g. ear protection.
Connection and commissioning	N/A	N/A	Risk of cutting/squashing when removing the product from the packaging and during mounting.	Grasp the housing and lift the product carefully out of the packaging. Avoid impact. Wear safety boots and cut-resistant gloves.
	N/A	N/A	Risk of damage to electronic components.	Use ESD protective equipment when mounting.
	Compliance with the electrical installation regulations	N/A		Observe the connection regulations that are valid in your country. (e.g. fusing, GFCI)

Transport

Only transport the product in its original packaging. Secure during transport. The vibration values, temperature and climate ranges should not be exceeded during transport.

Storage

Store the product in a dry and clean environment that is well protected. If the product is not operated for a longer period of time, we recommend running it for approx. 15 minutes annually to move the motor bearings.

Intended use includes:

- Operating the product with all protective equipment
- Do not put the product into operation before it has been installed in the customer's application
- Observation of the operating manual

The product is intended for use in sheltered rooms with controlled temperature and controlled humidity. Directly exposure to water must be avoided. Pollution degree 1 (according DIN EN 60664-1). There is either no pollution or it occurs only dry, non-conductive pollution. The pollution has no negative impact.

Ambient conditions

Table 14 Ambient conditions

Permitted ambient temperature	
Transport and storage	**Operation**

-40 °C ... 80 °C	-20 °C ... 75 °C

Voltage control

Speed control via the supply voltage is only permitted within the stipulated supply voltage range. Before connecting the product, ensure that the supply voltage corresponds with the product voltage. Check whether the data on the nameplate corresponds with the interface data. Only use cables that are designed for the current on the nameplate and the corresponding ambient conditions.

Vita

Paul Perez earned a bachelor's degree in mechanical engineering from the University of Texas at El Paso. During his undergraduate studies, he had the opportunity to be part of a Global & Regional Sustainable Engineering Program in Guadalajara, Mexico on which he worked on a binational engineering team to address sustainability issues and design a sustainable solution by developing a project that encourage the use of transportation and demonstrate its impacts to the public and creating a mobile application that provided useful (real-time) transportation information as other set of features. Since then he was also involved on research on different projects with the Center for Space Exploration and Technology Research and Texas Manufacturing Assistance Center. During his bachelor's degree, he started working as a teaching assistant for Introduction for Graphics and Design course and after he was enrolled on his master level took the roll for teaching assistant on Thermodynamics and Introduction to Thermal and Fluid and Science. During his bachelor's and master's degree he obtained a total of four scholarships, one fellowship, and three awards from his department. After graduating in fall 2017, Paul started his master's degree on Mechanical Engineering at the Czech Technical University and moved back to the University of Texas at El Paso, where he investigated Piezoelectric Sensors for flow measurements with high accuracy and fast response time. He determined the feasibility of using a piezoelectric as a velocity and flow rate sensor. Designed experiments to test piezoelectric sensors at ambient conditions and characterized and calibrated piezoelectric material sensors. Once graduating with his master's degree, Paul will use his expertise he acquired to achieve further success in the Industry.

Contact Information: paperez6@miners.utep.edu